“FEDERICO II”

UNIVERSITY OF NAPLES

SCHOOL OF MEDICINE AND SURGERY

DEPARTMENT OF TRANSLATIONAL MEDICAL SCIENCES

PhD Program
“Human Reproduction, Development and Growth”

Director
Prof. Claudio Pignata

PhD Thesis

“ANALYSIS OF MICRORNAs AS NOVEL BIOMARKERS IN LYSOSOMAL STORAGE DISEASES”

Tutor

Prof. Giancarlo Parenti

Student

Dr. AntoniettaTarallo

Academic Year 2014-2015

INDEX

General introduction

- Lysosomal storage diseases

The lysosomal storage diseases (LSDs) are a group of more than 50 inborn metabolic disorders. LSDs are caused by mutations in genes encoding soluble acidic hydrolases, integral membrane proteins, activator proteins, transporter proteins, or nonlysosomal proteins that are necessary for lysosomal function. Functional deficiencies in these proteins trigger a pathogenetic cascade that leads to intralysosomal accumulation of undegraded substrates in multiple tissues and organs. LSDs are traditionally classified according to the chemical properties of the accumulated substrate. Individually, each of these disorders is rare. However, their cumulative prevalence is relatively high when compared with other groups of rare diseases, and prevalence is estimated to be approximately 1 in 8,000 live births [Fuller M et al, 2006, Parenti et al, 2015].

LSDs are multisystem diseases and in most instances are highly debilitating, shorten patients' survival, and cause progressive physical and neurological handicaps. The clinical consequence of substrate storage in multiple organs and systems is the variable association of visceral, ocular, hematological, skeletal, and neurological manifestations, and there is partial phenotypic overlap among different disorders. Symptoms may emerge at variable ages, in some cases starting in utero or becoming evident in late adulthood. In general, the diseases progress and evolve over time.

LSDs are often responsible for physical and neurological disabilities, and they have impacts on patients' health and life expectancy. For all these reasons, caring for patients with LSDs requires a multidisciplinary approach. Although remarkable progress in treatment has been made in recent years, these disorders remain associated with important unmet medical needs and heavy burdens in terms of public health and economic costs [Parenti et al, 2015]. The past 25 years have been characterized by intensive and continual efforts to develop therapies specifically aimed at correcting the metabolic defects of these disorders. The approaches developed to treat LSDs are based on different strategies, each targeting a specific event in the pathogenetic cascade.

These approaches include strategies aimed at increasing the residual activity of a missing enzyme, as enzyme replacement therapy (ERT) [Brady, 2006], hematopoietic stem cell transplantation (HSCT) [Orchard et al, 2007], enzyme enhancement therapy (EET) by pharmacological chaperones [Fan, 2008] and gene therapy and approaches based on reducing the flux of substrates to lysosomes, as substrate reduction therapy (SRT) [Butters et al, 2005]. As knowledge has improved about the pathophysiology of lysosomal storage diseases, novel targets for therapy have been identified, and innovative treatment approaches are being developed. For many LSDs reliable markers of disease progression and treatment efficacy would be required.

In this thesis I have studied two models of lysosomal disorders, Pompe disease (PD) and Fabry disease (FD).

- Pompe disease

PD (glycogenosis type II) is a prototype of LSD in which several of these problems, related to ERT efficacy, were encountered both in clinical and in laboratory studies. PD is an autosomal recessive disorder, with an estimated incidence of 1:40,000 live births. Since the first description of PD by the Dutch pathologist Johannes C. Pompe in 1932 continuous progress has been made in the understanding of its biochemistry and genetics and in the characterization of its phenotypic spectrum [Hirschhorn and Reuser, 2001; van der Ploeg and Reuser, 2008].

PD is a metabolic myopathy caused by mutations of the *GAA* gene, resulting in functional deficiency of the lysosomal hydrolase acid α-glucosidase (GAA, acid maltase, E.C.3.2.1.20) [van der PLoeg et al, 2008].

The *GAA* gene, localized in 17q25.2-q25.3, consists of 20 exons spread over 28 kb of genomic sequence and encodes for a protein of 952 amino acids with a predicted molecular mass of 110 kDa [Hoefsloot et al, 1990]. The 110 kDa GAA protein synthesized in the endoplasmic reticulum is a precursor polypeptide, which undergoes N-glycan processing in the Golgi apparatus, and is proteolytically processed in the lysosomes into active isoforms of 76 and 70 kDa, through an intermediate molecular form of 95 kDa [Hoefsloot et al, 1990].

The mature enzyme hydrolyzes the alpha-1,4 and 1,6-glycosidic bonds of glycogen, releasing glucose units that are then transported across the lysosomal membrane by a specific carrier.

Being GAA deficiency ubiquitous, PD is a multisystemic disease with glycogen storage occurring in almost every tissue and cell type. However, disease manifestations are predominantly related to muscle involvement and heart and skeletal muscle are the major sites of pathology.

Different mutations of the GAA gene result in a wide phenotypic spectrum, with respect to age of onset of manifestations, rate of disease progression and variable association of symptoms. The different clinical forms of PD range from a devastating classic infantile phenotype, characterized by early onset, severe cardiomyopathy and early lethality, to intermediate phenotypes and late onset (childhood, juvenile or adult) forms in which cardiac involvement is absent or mild [Hirschhorn et al, 2001; Kishnani et al, 2004; , Slonim et al, 2000].

- Fabry disease

Fabry disease (FD, OMIM 301500, ORPHA324) is an X-linked metabolic disorder due to mutations in the *GLA* gene encoding the lysosomal hydrolase alpha-galactosidase A (alpha-Gal A, EC 3.2.1.22). Functional deficiency of alpha-Gal A results in storage of globotriaosylceramide (Gb3) and related neutral glycosphingolipids [Germain, 2010] in vascular endothelial cells, kidney cells, cardiomyocytes and neurons.

Progressive accumulation of globotriaosylceramide and related glycosphingolipids (galabiosylceramide) within lysosomes has been shown to trigger a cascade of events including cellular death, compromised energy metabolism, small vessel injury, channel dysfunction in endothelial cells, oxidative stress, impaired autophagosome maturation, tissue ischemia, and cardiac and renal tissue fibrosis [Germain, 2010]. This cascade of events leads to selective damage of the renal glomerular and tubular epithelial cells, the myocardial cells and valvular fibrocytes, neurons of the dorsal root ganglia and autonomic nervous system, as well as the endothelial, perithelial, and smooth muscle cells of the vascular system.

The initial signs and symptoms of FD emerge during childhood and

adolescence and typically include neuropathic pain crises, angiokeratomas, hypohidrosis, and gastrointestinal problems, including diarrhea, constipation, abdominal pain, nausea and vomiting. Disease progression in adulthood leads to progressive and potentially life-threatening manifestations, including renal failure, cardiomyopathy, premature myocardial infarctions, and stroke. Major organ involvement typically presents between the age of 20 and 30 years.
FD is one of the most common lysosomal storage diseases with an estimated prevalence of approximately 1 in 100,000 [Fuller et al, 2006; Germain, 2010]. However, this prevalence is likely underestimated. An Italian screening program in 37,104 male neonates demonstrated an incidence of alpha-Gal A deficiency of 1 in 3,100 males and of 1 in 4,600 males with known disease mutations [Spada et al, 2006]. Studies in selected populations, such as patients with unexplained left ventricular hypertrophy [Nakao et al, 1995; Elliott et al, 2011] or with renal failure [Nakao et al, 2003; Tanaka et al, 2005], indicate that because signs and symptoms of the disease are in most cases non-specific, FD patients are frequently misdiagnosed, and the correct diagnosis of FD may be delayed.

In this thesis, for both these disease models I have explored the potential of microRNAs (miRNAs) as new tool for understanding of the diseases pathophysiology and as new potential biomarkers to follow disease diagnosis, progression and follow up of patients.

- MicroRNAs (miRNAs): their role in health and disesase.

miRNAs are a growing class of small non-coding RNAs (ncRNA) that regulate gene expression by targeting messenger RNAs (mRNAs) for translational repression or transcript degradation [Bartel et al, 2004]. Mature, biologically-active miRNAs are ~22 nucleotides in length, and are processed from much longer primary transcripts by the RNAse enzymes Drosha and Dicer in the nucleus and cytoplasm, respectively [Bartel et al, 2004; Shukla et al, 2011]. miRNAs bind to complementary sequences usually located in the 3' untranslated region (UTR) of target genes and regulate post-transcriptionally their expression by reducing the stability and translational efficiency of their corresponding messenger RNA [Eulalio et al, 2008; Djuranovic et al, 2012;

Fabian et al, 2012]. To date, more than 2000 miRNAs have been identified in the human genome (miRBase version 19). It is estimated that a single miRNA may regulate hundreds of mRNAs and thus, has the potential to greatly impact gene expression networks [Bushati et al, 2007; Bartel et al, 2009; Pasquinelli et al, 2012]. In humans, deregulation of miRNAs is the hallmark of many diseases such as diabetes, neurodegenerative diseases, autoimmune conditions, heart failure and cancer among others [Mendell et al, 2012; Croce et al, 2009]. Remarkably, mutations in miRNAs have already been shown to play a primary pathogenic role in human genetic diseases, including inherited deafness [Mencia et al, 2009], keratoconus [Hughes et al, 2011] and skeletal abnormalities [de Pontual et al 2011].

Circulating miRNAs as disease biomarkers.

Recently, it has been shown that miRNAs can be exported from cells, loaded into lipid-rich vesicles called exosomes and transferred to neighboring or distant cells and parts of the body [Kinet et al, 2013]. Indeed, detectable levels of miRNAs exist in most extracellular biological fluids including plasma, serum, saliva, urine, tears, and breast milk [Kinet et al, 2013]. Circulating miRNAs exhibit high stability in serum and plasma samples and can be reliably measured [Mitchell et al, 2008]. miRNA signatures in blood appear to be tissue- and disease-specific and the miRNA content in circulation is likely to provide a read-out of altered pathways in response to disease conditions. Pioneering work from the cancer field has shown that miRNA expression profiles offer superior resolution compared to mRNA signatures for cancer subtype classification and prognosis [reviewed in Allegra et al, 2012]. Indeed, circulating miRNAs detected in cell-free serum can distinguish diseased individuals from healthy controls for a number of conditions. Considering that blood collection is the most common, convenient and non-invasive resource of biomarker testing, circulating miRNAs thus have a great potential as diagnostic, prognostic and predictive disease biomarkers. Obtaining indirect readouts of pathological processes is particularly important for certain disorders in which direct access to the affected tissue for molecular analyses is invasive.

There are several examples of alterations in the levels of circulating miRNAs associated with a disease condition. In cardiovascular disease, for instance,

levels of circulating miR-1, miR-133a and miR-208 can correlate with the severity of acute myocardial infarction [Kinet et al, 2013; D'Alessandra et al, 2010; Cheng et al, 2010; Wang et al, 2010; Kuwabara et al, 2011; Devaux 2012]. Circulating levels of miR-1, miR-133 and miR-206 have been shown to be new and valuable biomarkers for the diagnosis of Duchenne muscular dystrophy (DMD) and possibly also for monitoring the outcomes of therapeutic interventions in humans [Cacchiarelli et al, 2011]. Distinctive serum miRNA profiles have also been described for mouse models of striated muscular pathologies [Vignier et al, 2013]. In addition, characteristic circulating miRNA profiles have been reported for tissue injury and infection, physiological and psychiatric changes (such as pregnancy and bipolar mania [Gilad et al, 2008; Rong et al, 2011]. Interestingly, many individual studies claimed that circulating miRNA levels returned to baseline levels following treatment such as surgical removal of tumours, chemotherapy, acute myocardial infarction recovery and other medical treatments, further strengthening the role of circulating miRNAs as biomarkers monitoring the effectiveness of treatment [Ma et al, 2012; Cacchiarelli et al, 2011].

The potential of miRNAs as disease biomarkers has been further explored with the advancement and accessibility of next generation sequencing (NGS). NGS technologies have revolutionized our ability to characterize and quantify transcriptomes and provide a more precise measurement of transcript levels and their isoforms than microarray technology. State-of-the-art NGS enables high-throughput mRNA (RNA-seq) and small RNA analysis (Small RNA-seq) through direct sequencing and has a large dynamic range of detection with single base resolution that enables accurate quantification of transcript levels. Therefore, Small RNA-seq is currently considered the method of choice to effectively study miRNA expression.

<u>miRNAs as therapeutic targets.</u>

One of the most appealing properties of miRNAs is their ability to concurrently target multiple effectors of pathways in the context of a network, thereby regulating multiple cellular functions involved in disease development and progression. For this reason, targeting miRNAs for therapy is currently of great interest. The aberrant expression of a miRNA in disease can be modulated as a number of technologies to functionally inhibit or mimic

miRNAs already exist. Recent pre-clinical studies from the cancer field demonstrated the feasibility and efficacy of delivery of tumour suppressive miRNAs through miRNA mimics and inhibition of oncogenic miRNAs through delivery of antagomiRs and locked nucleic acid (LNA) molecules [reviewed in Ling et al, 2013]. In addition, there is currently an on-going clinical Phase II trial (NCT01872936) with miR-122 inhibitor (Miravirsen) for the patients infected with chronic hepatitis C virus. These studies highlight the potential of miRNAs to be used as drugs or drug targets in the near future.

Aim of the thesis

The general aim of the project of my thesis is to identify novel biomarkers for the treatment of LSDs, in particular Pompe disease, that may translate into improved efficacy of the existing therapies for these disorders.

Circulating miRNA profile can provide new/valuable biomarkers to monitor disease progression and the effects of therapeutic interventions.

Identification of specific differentially espressed miRNAs (DE-miRNAs) in tissues/organs that are primary targets of disease in these LSDs may be exploited to develop novel therapeutic approaches and monitor disease progression.

In vitro systems may provide reliable tools and read-outs to evaluate the effects of DE-miRNA modulation.

The analysis of miRNAs in these LSDs represents a way to address some of the unmet medical needs:

- Availability of markers of disease progression;
- Markers of ERT efficacy;
- Optimization of costs of therapies (ERT is highly expensive: 300.000-600.000 eu/year for a single patient);
- Possible identification of novel therapeutic targets.

The first aim of the project was focused on the analysis of circulating and tissues specific miRNAs in Pompe disease (PD). This study is in the final phase with the analysis of a large cohort of patients.

The second aim of this research project is focused on the analysis of circulating and tissue specific miRNAs in Fabry disease (FD). This study was performed on the animal model of FD and now is starting on patients.

Currently, I am also studying the mechanisms underlying the physiophatology of Pompe disease and its muscle damage.

Chapter 1

Analysis of circulating and tissue specific microRNAs in Pompe disease.

Introduction

Pompe disease and muscle involvement

The cascade of events that starting from glycogen storage, the hallmark of PD, lead to cell death and muscle atrophy and destruction is still poorly understood. For many years, since the identification of lysosomal storage diseases, it was assumed that storage "*per se*" was responsible for cell and tissue damage. In PD the rupture of glycogen-filled lysosomes was considered the major cause of muscle destruction. Only in the recent years studies have been conducted on the molecular and cellular mechanisms underlying the extensive disruption of the contractile apparatus in PD and suggesting that other factors are likely to concur in causing tissue damage.

Specifically, these studies addressed a number of questions, such as how atrophy and decreased performance contribute to functional insufficiency, and what are the cellular events and pathways that are activated by glycogen storage and account for morphologic and architectural changes. Elucidating these aspects is of great importance, not only for the knowledge of PD pathophysiology, but also because these mechanisms are potential targets of therapy.

Limited efficacy of ERT on skeletal muscle damage in PD

The last decade has witnessed extraordinary innovation in the treatment of PD. Until 2000 the management of PD patients was exclusively based on support treatment. For the strong impact of muscle insufficiency on the function of different organs and systems, the management of PD patients, like in many others genetic myopathies, requires a multidisciplinary team.

ERT with recombinant human GAA (rhGAA) is presently the only approved pharmacologic treatment to PD [Van den Hout et al, 2000].

ERT is based on the concept that recombinant lysosomal hydrolases, can be administered periodically to patients by an intravenous route. The enzymes are internalized by patients' cells and tissues through the mannose or mannose-6-phosphate receptor (MPR) pathways and are ultimately delivered to lysosomes, where they are activated and replace the function of the defective hydrolases. The presence of mannose-6-phosphate ligands in the

enzyme molecules and the integrity of the MPR pathway in the target cells and tissues are therefore crucial for the efficacy of this therapeutic approach.
The results of the published studies showed dramatic improvements of cardiac, respiratory and motor function in some patients, whereas in others ERT failed to cause significant clinical improvement [Kishnani et al, 2006; van Capelle et al, 2008]. This suggests that the clinical outcome in response to ERT may be variable, correlating with histological evidence of poor glycogen clearance [Thurberg et al, 2006], and that correction of glycogen storage in skeletal muscle is particularly challenging. Factors such as age at the start of treatment, stage of skeletal muscle damage, antibody responses [Amalfitano et al, 2001], insufficient targeting of rhGAA to skeletal muscle and high clearance of the enzyme by the liver [Raben et al, 2003] play a role in ERT efficacy, although the reasons for the variable responses of different PD patients are not completely clear and other factors, such as patients' genotype and abnormalities of cell functions, may also be implicated. The limitations of ERT, together with the high costs of this type of treatment (as much as several hundred thousand US dollars for each patient per year), point to the need for improved therapeutic strategies.

How to follow disease course and ERT efficacy?

A major issue in the monitoring of disease stage and therapeutic efficacy is the availability of objective and reliable tests that are not influenced by inter and intra-investigator variance. Widely used tests are the 6-minute walking test (6MW), tests that explore respiratory function (forced vital capacity, FVC; maximum inspiratory pressure, MIP; maximum expiratory pressure, MEP), tests exploring muscle function (quantitative muscle testing, MRC; timed muscle function tests; Rotterdam Handicap
Scale, RHS; Walton and Gardner-Medwin, WGM, etc), composite tests (Gait Stairs Chair Gower, GSCG), and tests evaluating limitations in physical activities and social participation (Rasch-designed Pompe-specific Activity scale, R-Pact). Although several of these tests have been validated for PD [Angelini et al, 2012; van der Beek et al, 2013], some of them some are specific for subsets of patients, require specific medical skills and collaboration of patients. Key factors in the evaluation of these tests are their

clinical relevance and the minimal clinically important difference that for some of these tests need to be further established [Lachman and Schoser, 2013].

Biochemical or imaging-based tests include the evaluation of the glucose tetrasaccharide (GLC4) [Young et al, 2009] in plasma and urine, muscle ultrasound [Vill et al, 2014], muscle NMR [Mercuri et al, 2002].

Also in these cases, however, the clinical relevance of the tests needs further assessment. Serial muscle biopsies do not appear to be a feasible approach to evaluate ERT efficacy as they require invasive procedures.

The availability of reliable tests appears even more important for the development of guidelines for the monitoring of patients, for ERT inclusion and exclusion criteria that are currently being identified in many countries [such as UK, and other European countries].

A set of reliable clinical and biochemical tests may also prove to be useful in optimizing ERT, and may in principle translate into economical benefits. They may also be precious tools in evaluating the efficacy of novel treatments or treatment protocols in comparison with existing therapies needs to be assessed.

Objectives

The scope of the project is to identify miRNAs that may serve as markers of disease progression and of efficacy of therapies, and to obtain information on the pathophysiology of PD. The availability of objective indicators, in combination with clinical evaluation, has clinical relevance and may help address important issues in the treatment and monitoring of PD patients.

The main aim of the project is to identify, by means of Next-Generation Sequencing (NGS)-based approaches, miRNAs acting as biomarkers in PD that may be translated into clinical relevant instruments enabling a more effective clinical management of patients. This effort could generate reliable diagnostic tools for PD that could be used to monitor the efficacy of ERT and provide information to optimize therapeutic interventions. Besides their value in identifying miRNA biomarkers, the generated data could provide insights into the complex mechanisms involved in the pathophysiology of PD, and into the functional role of miRNAs in the pathogenesis of the disease, possibly leading to the identification of new potential therapeutic targets.

Objective 1: Screening of differentially expressed miRNAs in the mouse model of PD

miRNAs expression profiles were analyzed by next generation sequencing (NGS) in target tissue/organs and plasma samples from the mouse model of PD in comparison to wild-type animals and at different time-points that were representative of different stages of disease progression.

The analysis was performed in tissues that were most relevant for the disease (heart and gastrocnemius) and in plasma from PD mice and age-matched wild-type mice. The tissues were collected at different time-points that correspond to different stages of disease progression and severity.

This analysis had the potential to identify circulating differentially expressed miRNAs (DE-miRNAs) that could be used as diagnostic biomarkers for PD and tissue specific DE-miRNAs that could be targeted as new therapeutic targets.

Results

We have analyzed miRNA profiles in plasma and tissues from PD mice with the aim to identify “disease-specific” miRNAs for PD. To have a general view of the overall detected and DE-miRNAs in the examined tissues, we performed the analysis by a NGS-by-synthesis approach, that allows the detection of even small differences among samples, and enables the identification of non-annotated miRNAs. NGS screening in the PD mouse model was performed at 3 and 9 months (two stages of disease progression).

Plasma and tissues were collected and total RNA was extracted by a procedure preserving small RNAs fraction. After small-RNA seq experiment, bioinformatics analysis was done to assess reliability and statistical relevance of data (FIGURE 1).

FIGURE 1

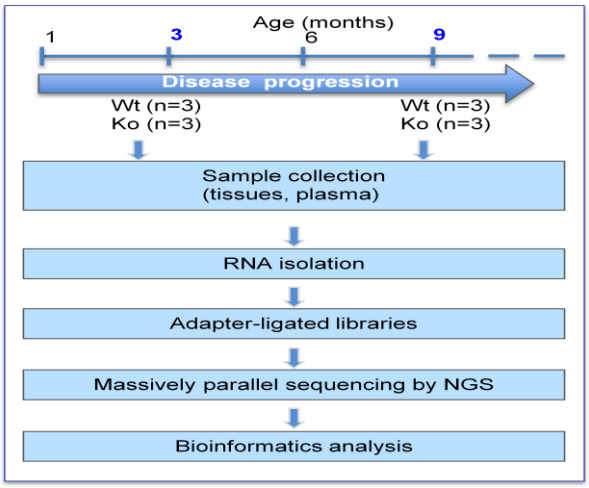

The analysis showed one DE-miRNA in plasma at time point of 9 months with statistical significance (FDR<0.05). In tissues we found 219 DE-miRNAs in muscle (gastrocnemius), and 35 DE-miRNAs in heart. In total, 104 miRNAs were differentially expressed at 3 months, 108 at 9 months; 42 were differentially expressed at both ages (FIGURE 2).

FIGURE 2

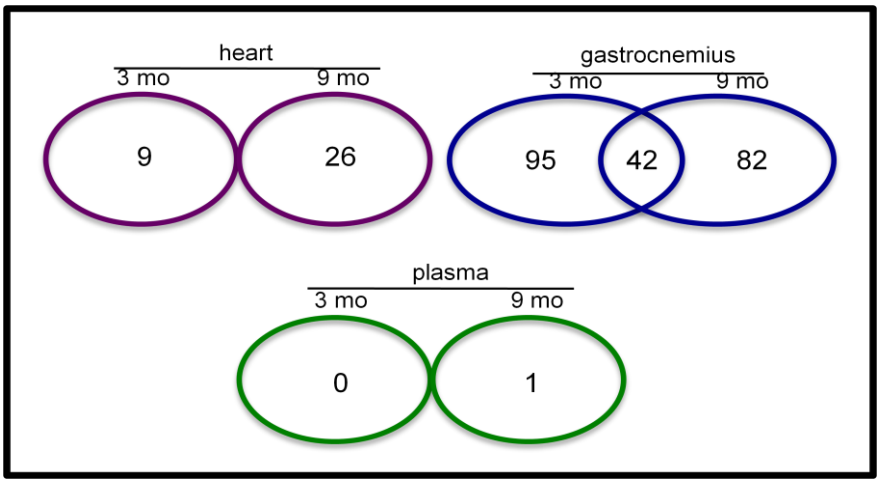

The NGS analysis generated a list of differentially expressed miRNAs in tissues representing the primary target organs of PD. This may represent a valuable framework to better understand the abnormalities of cellular pathways triggered by storage and associated with the pathogenesis of PD, and to identify candidates for therapeutic intervention. In the heatmaps

(FIGURE 3) are shown all the heart- and muscle-specific DE-miRNAs that we found by NGS. The colours show the levels of alteration of each DE-miRNA (in green downregulated miRNAs, in red upregulated miRNAs); the brillance of colours is proportionally to the grade of alteration.

FIGURE 3

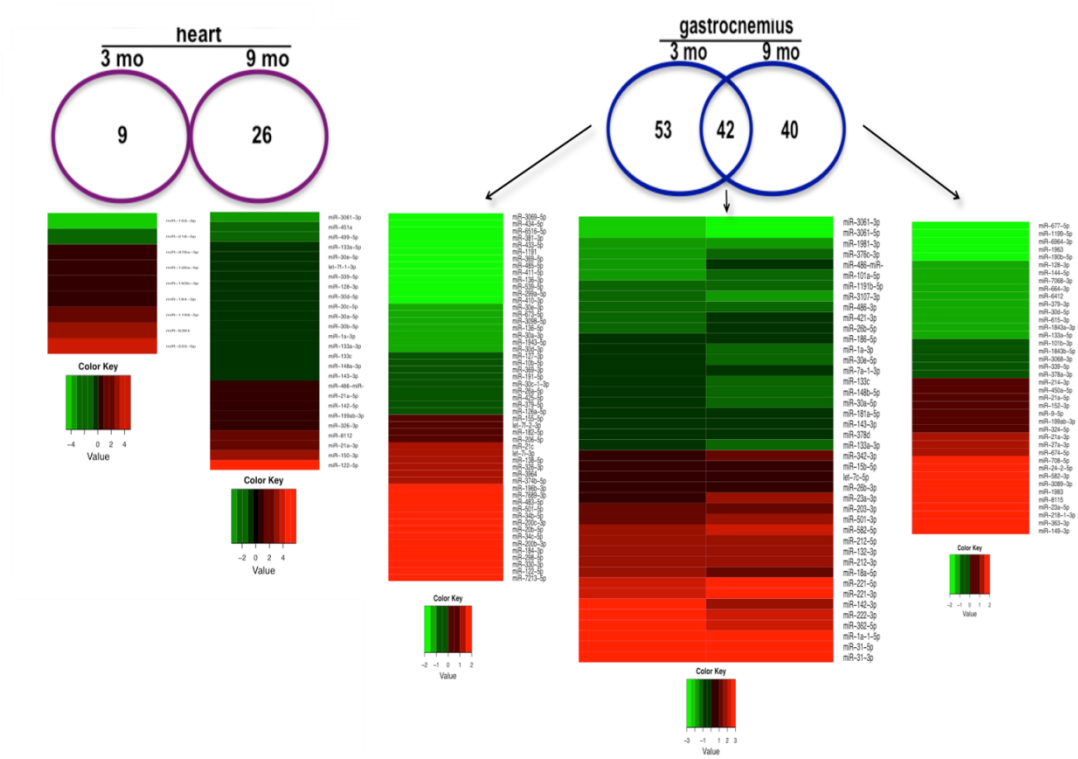

Objective 2: Assessment of diagnostic and/or predictive value of circulating DE-miRNA and tissues specific DE-miRNAs in the mouse model of PD by RealTime PCR (qRT-PCR)

2.1) miR-486 was differentially expressed in plasma of PD mice in comparison to wt mice at 9 months of age, with a highly significant FDR (<0.05).

miR-486 is already known because of its involvement in relevant processes for PD. miR-486 is a muscle enriched microRNA, is transcribed within the ANK1 gene (a small skeletal muscle-specific protein associated with the sarcoplasmic reticulum of skeletal muscle myofibers) [Zhou et al, 1997; Gallagher et al, 1998]

Its validated targets are important genes (Pax7, Foxo1, Pten) involved in pathways as myogenesis and atrophy, that are known to be altered in PD.
The expression of miR-486 is significantly reduced in dystrophin-deficient skeletal muscle; moreover, this miRNA is essential for normal myoblast fusion, cellular kinetics and viability and regulates a variety of PTEN/AKT signaling components in skeletal muscle [Alexander et al. 2011]
The miRNA expression data in plasma were validated by performing qRT-PCR for miR-486 in PD mice at different time points.

2.2) The results obtained obtained by NGS with some tissue-specific DE-miRNAs were also validated by performing qRT-PCR. These miRNAs were selected because of their highly significant FDR (< 0.05) or fold change, or due to their involvement in relevant processes for PD.
Some of these DE-miRNAs are already known to modulate the expression of genes involved in pathways such as autophagy, muscle regeneration, inflammation that may be relevant for PD pathophysiology. Some of them are known to modulate the expression of genes involved in more than one of these pathways.

Results

2.1) We first analyzed (by qRT-PCR) plasma from the PD mouse model at different ages and stages of disease progression; afterwards we moved to the study of human samples obtained from patients. We decided to use this approach because in the animal model we had a homogeneous situation with respect to phenotype, age of onset and progression of the disease.
We performed a time course of circulating miR-486 in PD mouse plasma at different time points (3, 6,12, 15, 18, months) to monitor the trend of this DE-miRNA during the course of disease progression (FIGURE 4).

FIGURE 4

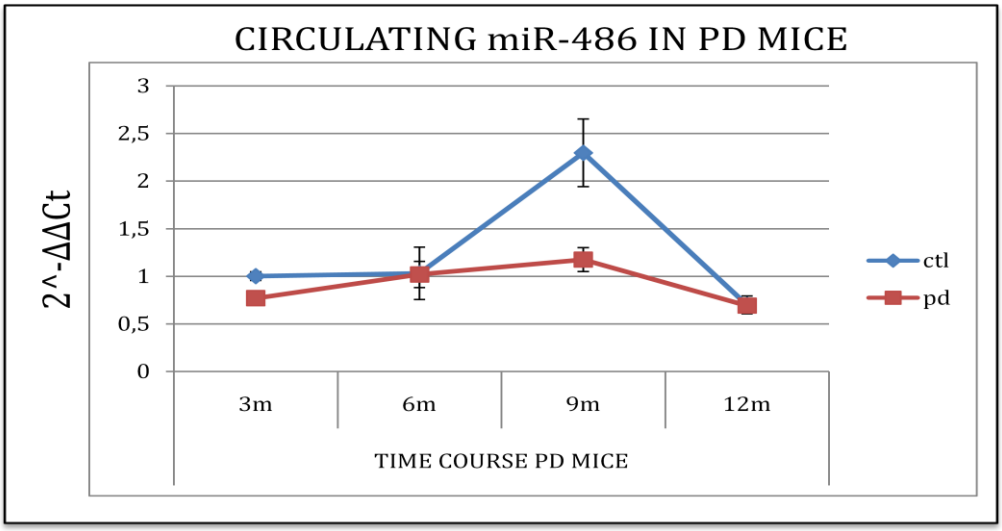

A cohort of 20 mice (10 wt and 10 PD) was followed since the age of 3 months. Blood samples were taken every three months to monitor miR-486 trend during disease progression. qRT-PCR data confirmed NGS data in plasma, even if they show a large variability among mice belonging to the same group. Like by NGS, at 3 months we did not see a substantial difference between wt and PD in the levels of circulating miR-486. At 9 months we observed a down-regulation of miR-486 in PD mice plasma *vs* wt, as already observed by NGS. The time-course analysis is still in progress at more advanced time points (15, 18, 21 months).

2.2) Some of the tissue specific DE-miRNAs have been selected for further evaluation and validation, based on the number of reads resulting by NGS and on their potential role. Indeed, some of them have already been reported in the literature and are known to modulate the expression of genes involved in pathways such as autophagy, muscle regeneration, inflammation that may be relevant for PD pathophysiology (FIGURE 5A). Some of them are also known to be implicated in more than one of these pathways. We firstly selected tissue specific DE-miRNAs that were more interesting for our pourpose, due to their implication in important pathways for PD, and because they are predicted to target relevant genes involved in important processes (FIGURE 5B).

FIGURE 5

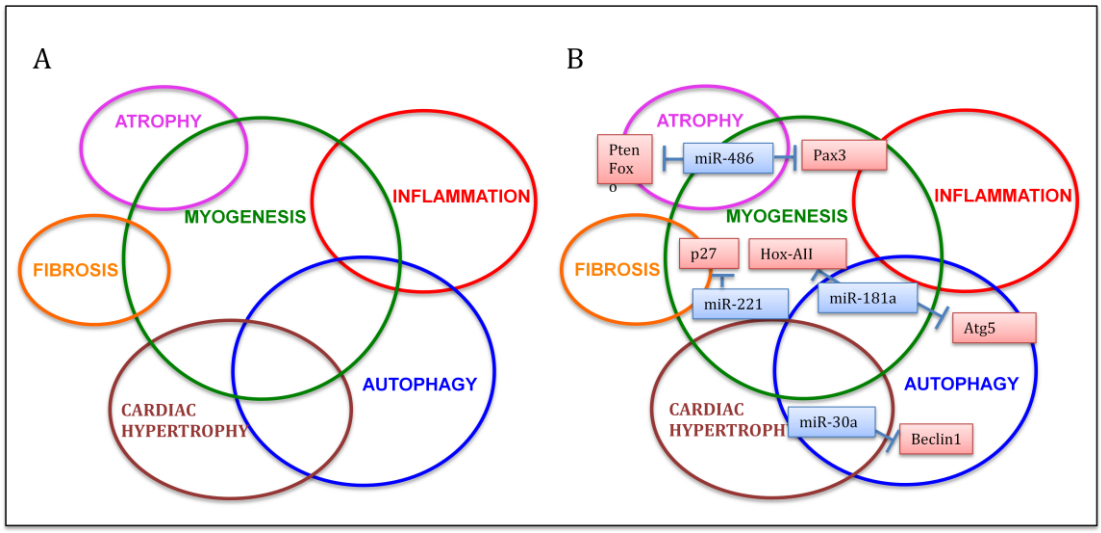

Also in this case, before proceeding with further experiments, we validated our data by means of q-RT-PCR.

We analyzed, in muscle (gastrocmenius) of PD mice at 9 months, some of DE-miRNAs selected over previously in figure 5b (FIGURE 6).

FIGURE 6

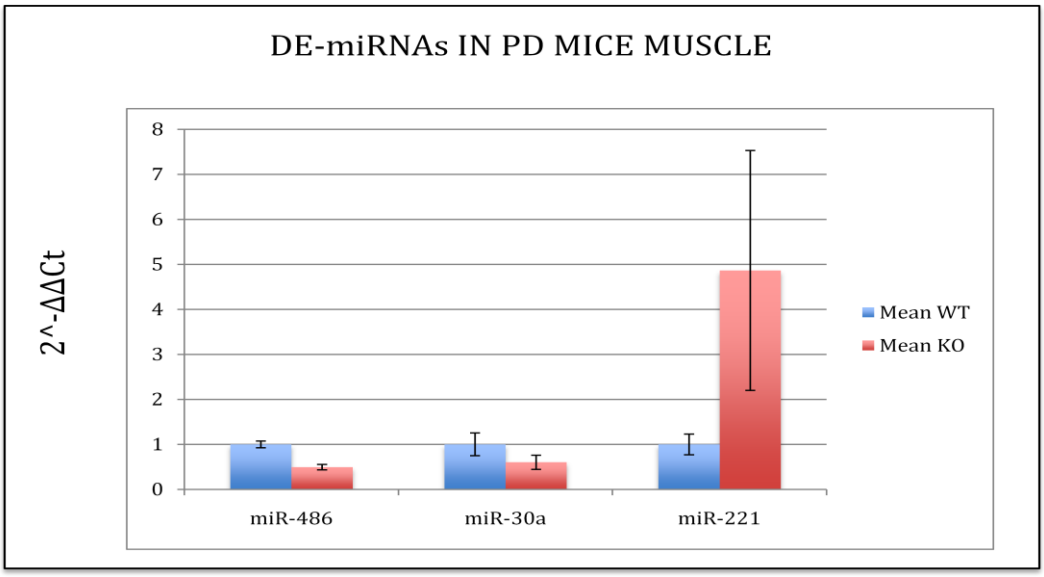

q-RT-PCR confirmed the NGS data trend of DE-miRNAs also in tissues. Therefore, we decided to adopt this method as gold standard for our future miRNA levels evaluation, because it is faster and less expensive, expecially when the attention is mainly focused on few miRNAs with respect to those

detected by massively parallel sequencing.

Objective 3: Assessment of diagnostic and/or predictive value of circulating DE-miRNA in plasma samples from a cohort of PD patients.

Monitoring miR-486 expression in combination with clinical evaluation, is clinically relevant for the follow-up of disease progression and therapeutic efficacy in PD patients. To this aim we contacted Italian Centers involved in the care of PD patients and started a collaborations with them.

Results

We analyzed plasma samples from 19 PD patients followed at DISMET, Naples at the Department of Neurology, University of Messina, and at the Department of Neurosciences, Federico II University, Naples. (Ten additional plasma samples of PD patients followed at Bambino Gesù Hospital, Rome and at the Centre for Rare Disease, Udine will be included in the study).

Plasma was obtained according to standard procedures during periodic follow-up admissions to the respective Hospitals. Peripheral blood was collected in EDTA and immediately processed, or stored at -80°C. Samples from age-matched controls were analyzed for comparison.

RNA was extracted (as described) and analyzed by qRT-PCR as indicated above. miR-486 levels were higher in PD samples compared to controls, both in early onset ($p<0.05$) (FIGURE 7A) and late onset (control samples insufficient for statistical analysis) PD patients (FIGURE 7B).

The overall trend showed that early onset patients had higher levels of circulating miR-486 with respect to late onset ones; this could be due either to the severity of disease or to a greater degree of atrophy in the infantile form of PD.

FIGURE 7

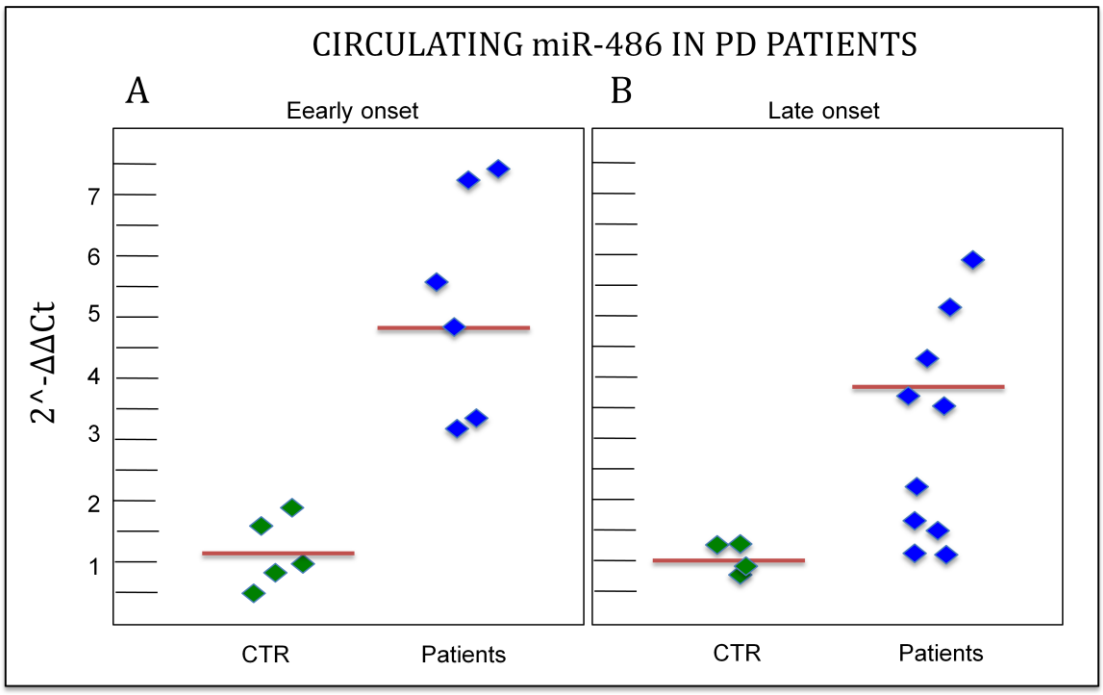

The broad variation in the plasma levels of different patients may in principle be due to a number of different factors. In this respect it should be noticed that patient phenotype, age, clinical forms, age of patients, age of onset of the disease and age at the start of ERT administration were non-homogeneous.

We are currently better analyzing our data on PD patients in comparison with age-matched wild type controls and we are also correlating our data with clinical info of the patients (reported in TABLES 1 - 2).

Clinical information on the patients was provided by the sending physicians. Specifically, information have been requested concerning:

- age, gender;
- phenotype and age at the onset of clinical manifestations (infantile classic, infantile non-classic, childhood-, juvenile-, adult-onset), age at diagnosis;
- on/off ERT, age at start of ERT, ERT doses and frequency;
- present clinical status with particular attention to motor function, respiratory function;
- collection of plasma samples (time elapsed from last ERT infusion).

TABLE 1

ADULT PATIENTS				
patient	age	sex	molecular analisys	Clinical phenotype
S.A.	26y	M	IVS - 13T>G + 2237G>A (pW746X)	mild
C.A.	35y	M	IVS1-13T>G c.2530_2541del	late onset
N.P.	45y	F	c.3113T>G + c. 1194+21194+23del	late onset
G.D.	46y	M	IVS1-13T>G c.1551+1G>C	late onset
C.G.	47y	F	IVS1-13T>G c.2530_2541del	late onset
C.G.	47y	M	c.32-13T>G + c.1124G>T	late onset
T.A.	48y	M	c.-32-13T>G c2481+102_2646+31del	late onset
B.A.	49y	M	IVS1-13T>G c.2395C>T	late onset
M.R.	54y	F	IVS1-13T>G c.1551+1G>C	late onset
N.A.	58y	M	c.3113T>G + c. 1194+21194+23del	late onset
B.R.	61y	F	IVS1-13T>G c.1561G>A	late onset
C.G.	62y	F	IVS1-13T>G c.1551+1G>C	late onset
B.G.	76y	M	IVS1-13T>G	late onset

TABLE 2

PEDIATRIC PATIENTS				
patient	age	sex	molecular analisys	Clinical phenotype
Z.E.	9 m	F	-	early onset
B.A.	2y 6m	M	c236_246del + c1655T>C	early onset
M.G.	15y	M	c1635T>C + IVS1_3C>A	mild
P.R.	16y	F	T1655C + T1655C	early onset
R.C.	16y	M	c.32-13T>G + c.1082C>G	late onset
L.T.	16y	F	IVS1-13T>G c.1802C>G	late onset

Additional information is needed to better understand which aspect of the PD is influenced by circulating miR-486 or *vice versa*. For instance, we are better investigating the time of ERT treatment (i.e. age at the start of ERT for each patients, how long they have been subject to the treatment, in which phase of ERT infusion the blood sampling has been done).

Objective 4: Analysis of the effects of ERT on circulating DE-miRNA in PD mouse model and in early onset PD patients

To gather more information on the changes in miR-486 levels in PD we have investigated its trend before and after ERT (with recombinant human alpha-

glucosidase, rh-GAA, Myozyme).This could help understand if there is a correlation between GAA levels and circulating miR-486 levels and if some variations may be observed after therapy with the recombinant enzyme. The analysis has been performed both in the PD mouse model and in a limited number of PD patients for which samples pre- and prost-treatment were available.

The results of these experiments could likely provide more information on the effects of ERT and on the expression of miRNAs and genes involved in pathways that are important for PD pathophysiology. The information obtained could be relevant for the treatment of PD patients and could indicate marker(s) to follow and optimize ERT in patients (in terms of frequency of infusions, doses, etc.).

Results

Only for some infantile patients, followed at our department of Pediatrics, we had the possibility to obtain blood samples before starting their periodic ERT (pre ERT) and the day after ERT infusion (24h post ERT).

FIGURE 8

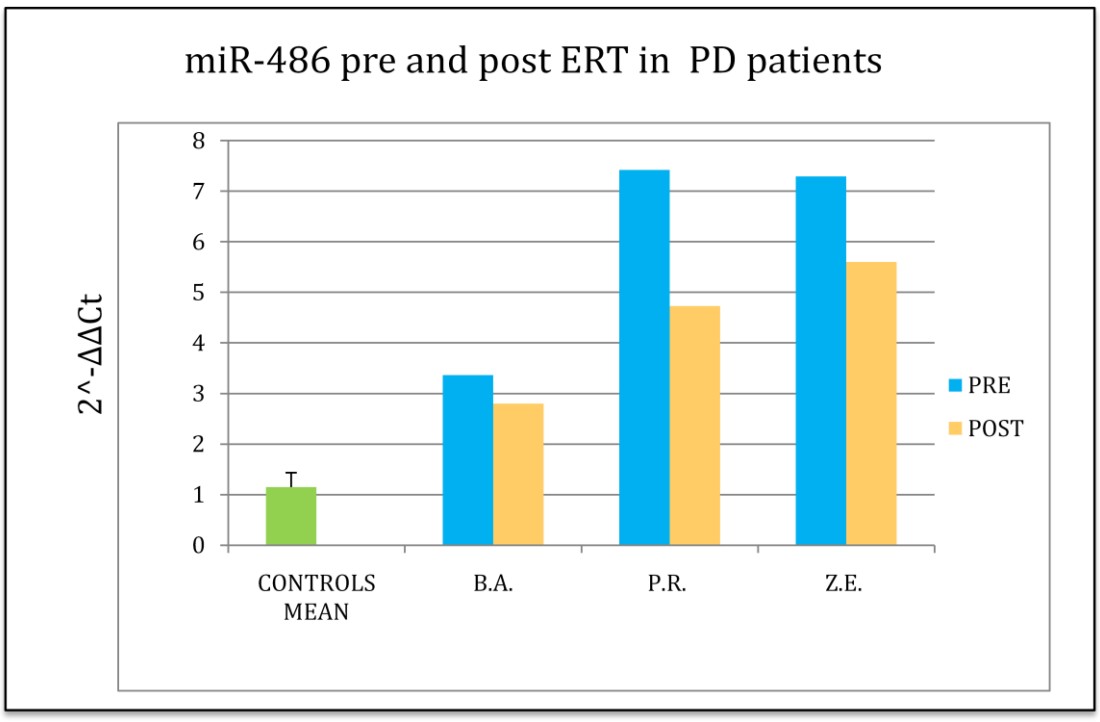

As shown in figure 8, all the 3 patients analyzed had up-regulated levels of miR-486 before ERT with respect to the mean of control samples. In each of these patients the level of miR-486 was lowered at 24 hrs post ERT. Although the patients are only 3, in all of them we found the same trend. Although we are aware that a wider cohort of patients is required to confer both statistical and biological strength to our findings, the observations obtained so far are indicative of a functional relationship between PD, ERT response and miR-486 deregulation.

We have also analyzed PD mice 9 months old, the age in which we found the most pronounced alteration of miR-486, even though with opposite trend with respect to PD patients.
Blood sampling of a group of wt control mice and PD mice was performed before ERT with recombinant enzyme (Myozyme) injection and 24h hours after injection.

FIGURE 9

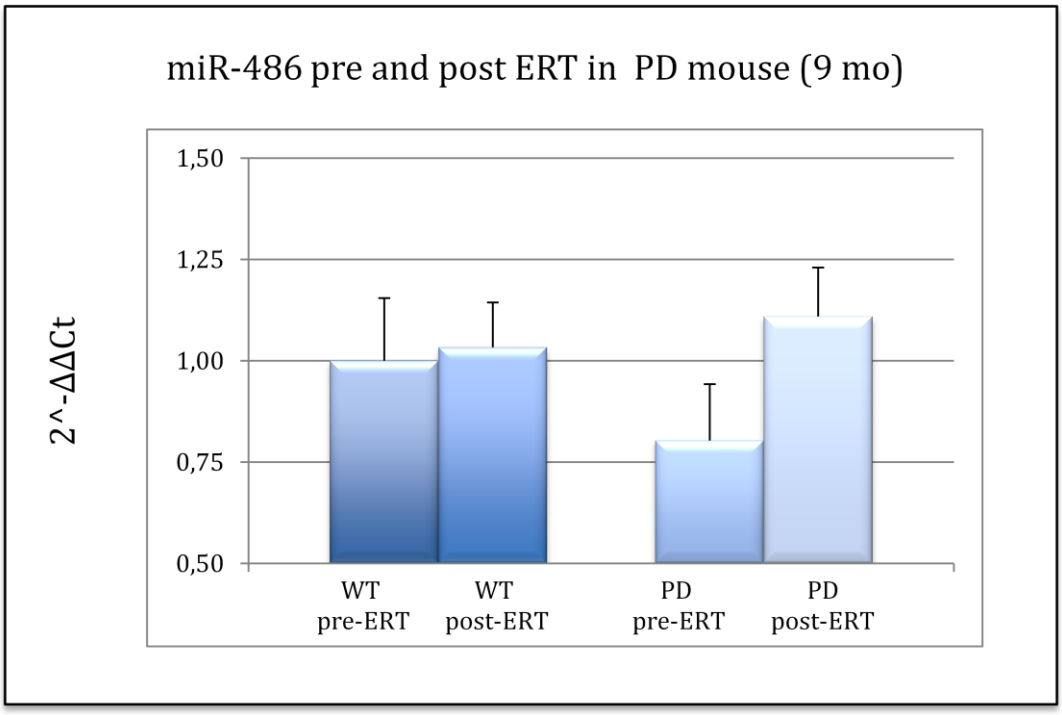

Before Myozyme injection, miR-486 level was down-regulated in PD mice in confront to control ones. After 24 hours of Myozyme injection, we found that miR-486 level in plasma rises (FIGURE 9).

In conclusion, although opposite with respect to patients, we found again a statistically relevant de-regulation of the investigated circulating miRNA in PD mouse, thus confirming a tight involvement of miR-486 in PD and suggesting that multiple factors may be implicated. On the other hand, the inversion of miRNA levels after ERT may indicate a rescue of one or more crucial pathway(s) targeted by miR-486, determined by the increased enzyme activity induced by ERT

Materials and methods

A KO Pompe disease mouse model obtained by insertion of neo into the *Gaa* gene exon 6 Raben et al, [1998] was purchased from Charles River Laboratories (Wilmington, MA), and is currently maintained at the Cardarelli Hospital's Animal Facility (Naples, Italy).

Animal studies were performed according to the EU Directive 86/609, regarding the protection of animals used for experimental purposes. Every procedure on the mice were performed with the aim of ensuring that discomfort, distress, pain, and injury would be minimal. Mice were euthanized following ketamine xylazine anesthesia.

Human PD fibroblasts (approximately 30 cell lines) and myoblasts (5 cell lines) are already available at the cell bank of the Department of Translational Medical Sciences (DISMET), Section of Pediatrics,

Federico II University, Naples.

Plasma samples were collected from 17 PD patients followed at DISMET, Naples at the Department of Neurology, University of Messina, and at the Department of Neurosciences, Federico II University, Naples. Plasma was obtained according to standard procedures during periodic follow-up admissions to the respective Hospital. Five ml of peripheral blood was collected in EDTA and immediately processed, or stored at -80°C. Samples from age-matched controls were analyzed for comparison.

Nine muscle biopsy samples are already available at DISMET (kindly provided by Prof. Antonio Toscano, Dept. of Neurology, University of Messina, and by Prof. Lucio Santoro, Dept. of Neurosciences, Federico II University, Naples). The samples have been obtained for diagnostic purposes and

patients have consented to their storage and use for research.

Total RNA extraction preserving miRNA fraction.

The methodology for extraction and analysis is already established in our laboratories.

Tissue samples were immediately submerged in RNA Stabilization Reagent (RNA later; QIAGEN), to stabilize RNA and preserve the gene expression profile, and frozen. Total RNA, including small RNAs, was extracted using the miRNeasy Kit (Qiagen) following the manufacturer's instructions. RNA was quantified using a NanoDrop ND-8000 spectrophotometer (NanoDrop Technologies) and the integrity was evaluated using an RNA 6000 Nano chip on a Bioanalyzer (Agilent Technologies). Only samples with an RNA integrity number (RIN)>8.0 were used for library preparation.

Small RNA-seq analysis in tissues

Small RNA libraries were constructed using a Truseq small RNA sample preparation kit (Illumina) following the manufacturer's protocol. Using multiplexing, we combined up to 12 samples into a single lane in order to obtain sufficient coverage. Equal volumes of the samples that constituted each library were pooled together immediately prior to gel purification and the 147-157 bp products from the pooled indexes were purified from a 6% polyacrylamide gel (Invitrogen). Libraries have been quality-checked using a DNA 1000 chip on a Bioanalyzer (Agilent Technologies) and quantified using the Qubit® 2.0 Fluorometer (Invitrogen).

Small RNA-seq analysis in plasma

For the analysis of circulating miRNA, we collected plasma from PD mice and age-matched wild-type mice by centrifugation of blood in serological tubes. For the preparation of plasma, EDTA was used as anticoagulant. Every effort was made to limit pre-analytical variation that could affect miRNA quantification. For instance, particular attention was given to prevent hemolysis. We monitored the levels of the granulocyte-specific miR-223 to assess the extent of hemolysis in the collected samples. All downstream processing of plasma samples from PD and control sets were conducted simultaneously to minimize

batch effect. Prior to RNA extraction, a *C. elegans*-specific synthetic exogenous miRNA (ce-miR-39) was spiked in the samples as control for the extraction efficiency. RNA was isolated using the miRNeasy Kit (Qiagen) and RT-PCR was performed using miScript System (Qiagen). RNA recovery was assessed by comparing the Ct values (obtained with the assay targeting the synthetic miRNA) with a standard curve of the synthetic miRNA generated independently of the RNA purification procedure. After the assessment of RNA recovery, equal amounts based on starting volume (3 μl) were used for the preparation of small RNA libraries, as previously described for tissue samples.

The sequencing was carried out by the NGS Core Facility at TIGEM, Naples. Cluster generation was performed on a Flow Cell v3 (TruSeq SR Cluster Kit v3; Illumina) using cBOT and sequencing was performed on the Illumina HiSeq1000 platform, according to the manufacturer's protocol. Each library was loaded at a concentration of 10 pM, which we had previously established as optimal.

Bioinformatics Analysis

To identify differentially expressed miRNAs (DE-miRNAs) across samples, the raw data were analyzed with the support of the Bioinformatics and Statistics Core Facility, TIGEM, Naples. Briefly, the reads were trimmed to remove adapter sequences and low quality ends, and reads mapping to contaminating sequences (e.g. ribosomal RNA, phIX control) were filtered-out. The filtered reads were aligned in parallel both to the mouse genome (mm10) and to mouse mature miRNAs (miRBase Release 20) using the CASAVA software (Illumina). The number of reads for each miRNA was normalised using Trimmed Mean of MS (TMM). The comparative analysis of miRNA levels across samples was performed with edgeR, a statistical package based on generalized linear models, suitable for multifactorial experiments.

The potential role, the target genes, and the pathways in which DE-miRNA identified by NGS were involved, were studied by bioinformatics tools (Gene Ontology, KEGG frequencies) and literature-based analysis (PubMed).

Quantitative Real-time Reverse-transcription Polymerase Chain Reaction (qRT-PCR) of miRNA and of specific target genes.

Expression of mature miRNAs were assayed using Taqman MicroRNA Assay (Applied Biosystems) specific for each miRNA selected for validation. qRT-PCR was performed by using an Applied Biosystems 7900 Real-time PCR System and a TaqMan Universal PCR Master Mix. All the primers for selected miRNAs were obtained from the TaqMan miRNA Assays. Samples were run in triplicate and small nuclear U6 snRNA and miR-16 (Applied Biosystems) were used as internal controls.

Differences in miRNAs expression, expressed as fold-changes, were calculated using the 2-DDCt method. To validate the target genes expression data, qRT-PCR was performed for selected target genes of some miRNAs. GAPDH, was used as endogenous reference transcript. The levels of selected target genes were measured by qRT-PCR using the LightCycler 480 (Roche) and specific forward and reverse primers for each target gene. The PCRs with cDNA were carried out in a total volume of 20 µl, using 10 µl LightCycler 480 SYBR Green I Master Mix (Roche) and 400nM specific primers under specific conditions that were validated for each of the genes analyzed. All the reactions were normalized against murine or human GAPDH. Each sample was analyzed in duplicate in two-independent experiments.

In vivo experiments on PD mouse model

PD ko mice received single injection of Myozyme into the retro-orbital vein (doses: 40 mg/kg; 100 mg/kg). The dose of 40 mg/kg corresponds to the dose used in human therapy. Plasma and tissue (heart, gastrocnemius) were collected 24 hrs or 48 hrs after the infusion and selected miRNA and mRNAs were analyzed by qRT-PCR as indicated. The results were compared with those obtained in untreated animals. For each group (treated, untreated, different time points) 5 animals were tested.

Conclusive remarks

LSDs, including PD, represent a group of invalidating pathologies with a strong impact on patients' life expectancy.

While remarkable progress in treatment has been made in recent years, the molecular mechanisms responsible for the phenotypic manifestations of these diseases and the key regulators of the functional pathways involved are still to be clarified. Given the increasing relevance conferred to small RNA molecules in human disease, also including neuromuscular disorders, we have studied the possible role of miRNA deregulation in PD. To globally characterize PD-specific miRNA expression profiles, we first applied a NGS approach, a new generation technology, quantitative and highly sensitive and more reliable if compared to hybridization-based methods.

This represents a versatile method since it can be applied to multiple experimental models, including animal ones, where this approach has been widely adopted also due to the homogeneous background of this model. Moreover, massively parallel sequencing allows, contrary to other high-throughput technologies, the identification of novel molecules that are still not annotated in public databases.

By performing small RNA sequencing of PD tissues and plasma samples isolated from PD mice, we identified several DE-miRNAs in tissues and one DE-miRNA in plasma, with respect to healthy mice.

This finding is somehow expected, particularly because of the known difficulties in miRNA purification from plasma, where these molecules are less stable and more subjected to degradation by RNAses compared to tissue samples. On the other hand, it results really challenging to observe reliable differences in plasma, since the identified factors are the results of multiple body parameters (Functions?) in a given moment.

Some of DE-miRNAs have already been reported in the literature and are known to modulate the expression of genes involved in pathways such as autophagy, muscle regeneration, inflammation, atrophy, that are relevant for PD pathophysiology. These results confirm the accuracy of the approach.

In plasma we found just one DE-miRNA, but with a great impact for its involvement in atrophy and myogenesys, crucial pathways for PD. In early onset patients we found more pronounced abnormalities of mi-486 levels, likely correlated with disease progression and severity. It is reasonable to speculate that miR486 is potentially useful as a biomarker, that may be monitored by using non-invasive approaches (blood sampling).

Our results are promising but there is a need for further evaluation in other samples. To this end international collaborations and multicenter coordinated actions have already been established.
Specifically, some relevant requests have been made to collaborating centres concerning higher number of plasma samples (PD patients and healty controls). We are doing an accurate study of correlation with clinical information of patients concerning:
- age, gender;
- phenotype and age at the onset of clinical manifestations, age at diagnosis;
- on/off ERT, age at start of ERT, ERT doses and frequency;
- present clinical status with particular attention to motor function, respiratory function;
- collection of plasma samples (time elapsed from last ERT infusion).

A circulating miRNA that is differentially expressed in the mouse model of PD has already been identified at the time point 9 months, but the NGS analysis at different time points, particularly in more advanced stages of disease (14 months and 21 months) is in progress. This might result in the identification of additional circulating DE-miRNAs.
As previously stated the availability of biochemical indicators, in combination with clinical evaluation, has clinical relevance for the monitoring of disease progression and therapeutic efficacy in PD patients.

Ongoing objectives

Objective 1: NGS analysis at more advanced stages of disease (14 months and 21 months)

Objective 2: Assessment of diagnostic and/or predictive value of tissue

specific DE-miRNAs and specific target genes in PD mouse model muscle and in PD patients muscle biopsies.

Objective 3: Analysis of selected DE-miRNAs in mouse- and patient-derived cells (mouse fibroblasts and myoblasts, patients fibroblasts and myoblasts, patients) *in vitro*. Cultured cells may represent a valuable tool to study in vitro the effects of ERT, on miRNA profiling and on specific pathways.

Chapter 2

Analysis of circulating and tissue specific microRNAs in Fabry disease.

Introduction

Because many manifestations of the disease are highly debilitating, FD imposes a heavy burden on public health, in terms of economical investments and need for assistance to patients and their families [Wyatt et al, 2012]. The treatment of morbidity associated with FD often requires invasive procedures (e.g. dialysis). Some FD manifestations, such as stroke, myocardial infarction, may result in physical handicap.

Therapies for Fabry disease

Until the beginning of the 2000s the management of FD patients was exclusively based on supportive therapies. In 2001, enzyme replacement therapy (ERT) with recombinant human alpha-galactosidase A (rh-alpha-Gal A) was introduced to treat FD [Eng et al, 2001; Schiffmann et al, 2001]. Two recombinant rh-alpha-Gal A preparations are presently approved in Europe for ERT, agalsidase alpha (Replagal, Shire), and agalsidase beta (Fabrazyme, Genzyme Co). ERT has been shown to promote substrate clearance from vascular endothelia and clinical improvement or stabilization of patients [Metha et al, 2009; Pisani et al, 2012].

In recent years pharmacological chaperone therapy has been proposed as an alternative or complementary approach to treat FD [Fan et al, 1999] and other lysosomal storage diseases [Parenti el al, 2009]. This approach is based on the use of active site-directed ligands (so called “chaperones”) that can provide protection against misfolding and prevent the degradation of mutated proteins with altered conformations. Chaperones have also been shown to act synergistically with ERT in FD [Porto et al, 2009; Porto et al, 2012; Pisani et al, 2012; Benjamin et al, 2012].

Other genetic therapies are being considered for the treatment of Fabry disease, such as substrate reduction therapy, *GLA* promoter activation, protein homeostasis regulation, next generation ERT, and gene therapy.

Open questions and unmet medical needs

Despite extraordinary progress in the treatment of FD, mainly achieved with the introduction of ERT, several issues remain to be addressed and unmet medical needs remain associated with this disorder.

1. *Clinical efficacy of ERT.* There is some evidence that substrate clearance by ERT in specific cell types and tissues is less efficient than in other cells. Recent meta-analyses indicated that, while significant clinical benefits of ERT have been obtained in some patients (mainly at an early phase of the disease), data that support the long-term clinical benefits of ERT are less solid [Schaefer et al, 2009; Lidove et al, 2010; Rombach et al, 2013]. Although evidence has been provided for an association between time on ERT and a decrease in left ventricular mass index and increase in the glomerular filtration rate in adults after adjustment for age, the magnitude of the differences is small [Wyatt et al, 2012]. The effect of treatment on glomerular filtration rate appears to plateau after 5 or 6 years on treatment. In some patients long term ERT does not prevent disease progression. Although the overall risk of developing complications declines with increasing treatment duration, in patients with advanced FD a significant risk may persist despite ERT [Weidemann et al, 2013].

2. When to start treatment? Which patients to treat? Recommendations for ERT in patients with FD have been published, and national guidelines exist in some countries. These guidelines, however, remain a matter of debate particularly when considering indications to start treatment in heterozygous female and children, and the appropriate time to start therapy in adult males in order to prevent irreversible organ damage. A Consensus Conference on FD nephropathy suggests that ERT should start at the onset of symptoms in women and at 7–10 years of age in asymptomatic boys [Lidove et al, 2007]. Data from the FD outcome survey (FOS) on the basis of clinical results of ERT and of its adverse effects, suggest that in asymptomatic children a close clinical surveillance should be performed, mostly in patients with a family history of early disease progression.

3. How to follow disease course and ERT efficacy? The efficacy of ERT is commonly followed on the basis of clinical and functional measures (progression of cardiac, renal or cerebral disease, glomerular filtration rate, pain). Biochemical markers that may assist with treatment monitoring include globotriaosylceramide and lysoglobotriaosylceramide measured in plasma and urine, and anti-agalsidase antibodies. However, substrate levels can be difficult to correlate with organ involvement or long-term disease progression in females and individuals not affected by the classic form of FD [Germain, 2010]. Current efforts are directed towards the identification of additional biochemical markers by metabolomic approaches [Dupont et al, 2012; Manwaring et al, 2013; Lavoie et al, 2013].

Objective

The second aim of my thesis is focused on the identification, by means of Next-Generation Sequencing (NGS)-based approaches, microRNAs (miRNAs) acting as biomarkers in FD that could be translated into clinical relevant instruments enabling a more effective clinical management of patients.

This effort could generate reliable diagnostic tools for FD that could be used to monitor the efficacy of ERT and provide information to optimize therapeutic interventions.

Besides their value in identifying miRNA biomarkers, the generated data could provide insights into the complex mechanisms involved in the pathophysiology of FD, and into the functional role of miRNAs in the pathogenesis of the disease, possibly leading to the identification of potential therapeutic targets.

The analysis of miRNAs in the animal model of FD represents a way to address some of the unmet medical needs (e.g. reliable biomarkers, need for new therapeutic targets) and provide a better understanding of the disease pathophysiology.

The circulating miRNA profile can provide new and valuable biomarkers to monitor the clinical course of patients, including the early stages of the disease, and the outcomes of therapeutic interventions.

In addition, the differential expression of FD-specific miRNAs in the tissues/organs that are primarily targeted in the course of the disease could be used as a point of intervention for novel therapeutic approaches.

Objective 1: Screening of differentially expressed miRNAs in the mouse model of Fabry disease.

miRNAs expression profiles were analyzed by next generation sequencing (NGS) in target tissue/organs and plasma samples from the mouse model of FD in comparison to wild-type animals and at one time-points that were representative of different stages of disease progression.

The analysis was performed in tissues that were most relevant for the disease (heart and kydney) and in plasma from FD mice and age-matched wild-type mice.

This analysis had the potential to identify circulating differentially expressed miRNAs (DE-miRNAs) that can be used as diagnostic biomarkers for FD.

Results

As done for Pompe disease, we have performed pilot, proof-of-principle experiments of miRNA profiling in plasma and tissue samples from FD and wild-type mice with the aim to validate our procedure for the identification of “disease-specific” miRNAs in FD. We have studied circulating and tissue miRNAs in the animal model of the disease.

Briefly, we have extracted total RNA from kidney, heart and plasma of the FD mouse model at 6 months of age, which represents an early stage of disease course. To account for variation in the miRNA contents due to technical and biological variability, we harvested our samples from 3 different, age-matched mice. Small RNA-Seq libraries were prepared as described previously.

Overall, by pooling and sequencing 12 samples per lane we could obtain a very good coverage for all miRNAs per sample (a total of 373,946,175 raw single-end reads per library and a sufficient average of 17,365,764 mappable reads per tissue sample and 27,592,835 mappable reads per plasma sample).

A list of the differentially expressed miRNAs (FDR< 0.05) that were identified after comparative analysis is summarized in the table below.

FABRY DISEASE mouse model

HEART

miRNA ID	logFC	FDR
mmu-miR-378a-3p	-0.243938198	1.11E-05
mmu-miR-126a-5p	-0.196726546	0.000382356
mmu-miR-182-5p	1.38554331	0.001662842
mmu-miR-486-mmu-miR-3107-5p	-0.275621891	0.005104922
mmu-miR-431-3p	-4.635581466	0.059900045

KIDNEY

miRNA ID	logFC	FDR
mmu-miR-1948-3p	6.489832007	0.015984727

PLASMA

miRNA ID	logFC	FDR
mmu-miR-96-5p	4.604963874	0.105568263

From these preliminary data we found that 6 miRNAs appear to be differentially expressed with statistical significance (FDR< 0.05) in FD mouse tissues with respect to age-matched control mice.

It is possible to speculate that the subset of differentially expressed miRNAs might increase with both the progression of disease and age. This has been already observed in the mouse model of another lysosomal storage disease (Pompe Disease, due to alpha-glucosidase deficiency), investigated at different ages by our group (unpublished confidential data). In that case we found, particularly in heart, a greater number of differentially expressed miRNAs at 9 months, when compared to 3-month-old mice.

Among all tissue and plasma FD samples investigated, we found four down-regulated miRNAs, whereas two were up-regulated. In plasma we didn't find circulating miRNAs differentially expressed with FDR <0.05, but we are investigating FD mouse model at more advantaged stages and ages of the disease.

Ongoing objectives

Objective 2: Identification of circulating miRNA profiles in the plasma of the mouse model of FD at different stages of disease progression and severity.

This specific objective aims at a) identifying miRNAs that are differentially expressed in the plasma of the FD mouse model compared to wild-type mice and b) establishing a circulating miRNA profile at different stages of disease progression.

To this end, we will harvest plasma from FD mice and age-matched wild-type mice by centrifugation of blood in serological tubes.

This analysis has the potential to identify circulating miRNAs that can be used as diagnostic biomarkers for FD even at very early / pre-symptomatic stages of the disease. The analysis of FD mice at different time-points of disease severity will also enable us to correlate circulating miRNA profiles in the FD mouse with clinical parameters of disease manifestation, and with involvement of specific organs.

Objective 3: Evaluate whether the selected miRNAs are differentially expressed also in samples from a cohort of FD patients

This part of the scientific program aims to identify miRNAs that are differentially expressed in the plasma from FD patients compared to 5 volunteer age-matched healthy individuals, and determine to what extent the circulating miRNA profiles of FD patients overlap with the ones detected in the FD mouse model.

Towards this end, we will analyze plasma samples obtained from a total of 40 patients (Table 2) that are followed at the Department of Public Health, Section of Nephrology, Federico II University, Naples, Italy.

In all patients the diagnosis was based on the clinical presentation, alpha-Gal A deficiency, and molecular characterization of *GLA* gene mutations.

Thirty-two (16 males -16 females) of these patients are currently under ERT, whereas 8 are untreated (4 males - 4 females).

Patients will be classified according to disease severity and progression by the Fabry Outcome Survey-Mainz Severity Score Index (FOS-MSSI) [Whybra et al, 2006]. The patients will also be classified for treatment duration.

Table 2

Patient	sex	Max score	Score				
			General	Neuro	Cardio	Renal	Total
ERT-treated							
1	m	Cardiac	7	5	18	15	45
2	m	General	9	4	10	10	33
3	f	General	8	3	7	5	23
4	f	Renal	5	3	5	10	23
5	m	Cardiac	5	4	15	6	30
6	f	General	8	8	8	8	32
7	f	Cardiac	5	5	14	6	30
8	f	Renal	5	5	10	15	35
9	m	General	10	5	10	10	35
10	m	Cardiac	7	5	15	10	37
11	m	General	10	5	6	6	27
12	m	Renal	5	5	10	15	35
13	f	General	10	5	8	7	30
14	m	Cardiac	5	5	15	8	33
15	m	General	10	3	10	10	33
16	m	General	10	5	12	12	39
17	f	General	10	5	15	10	40
18	m	General	10	5	15	15	45
19	m	Cardiac	10	5	20	15	50
20	f	Cardiac	10	5	18	10	43
21	f	Cardiac	8	5	18	10	41
22	m	General	10	10	10	10	40
23	f	Renal	10	5	10	15	40
24	m	General	10	10	10	10	40
25	m	Renal	10	10	10	15	45
26	f	General	10	10	10	10	40
27	f	General	10	10	10	10	40
28	f	General	10	10	10	10	40
29	f	Renal	10	5	10	15	40
30	f	Cardiac	10	5	18	10	43
31	f	Cardiac	10	5	18	10	43
32	m	Renal	10	10	10	15	45
Untreated							
33	f	General	8	3	7	5	23
34	f	Renal	5	3	5	10	23
35	m	Cardiac	5	4	13	6	28
36	f	General	8	8	8	8	32
37	m	Cardiac	5	5	14	6	30
38	f	Renal	5	5	10	10	30
39	m	General	10	5	10	10	35
40	m	Cardiac	7	5	12	10	35

To identify putative miRNA biomarkers in FD patients we will implement a screening strategy composed of two successive steps.

In the first step we will perform a small RNA-Seq profiling of plasma following the previously described protocol in a small subset (n=5) of patients with advanced stage FD.

The second step will consist in the validation of a sub-set of miRNAs identified both from the analysis of patients and of the FD mouse in the whole cohort of FD patients (n=40, see above) using Quantitative (q) Reverse Transcriptase (RT-) PCR (qRT-PCR) miRNA profiling.

Materials and methods

A FD knockout mouse model was purchased form Jackson laboratories and is available in our laboratory. FD knockout mouse model was generated by introducing a 1 kb deletion into the *GLA* gene, spanning part of exon III and intron III. The mouse model completely lacks alpha-Gal A and shows the pathologic features of FD, with accumulation of substrates in the kidneys, liver, and in cultured fibroblasts. Ultrastructural analysis reveals concentric lamellar inclusions in kidneys. The FD mouse model has been purchased from Jackson Labs and is already available in our laboratory.

A total of 40 patients followed at the Department of Public Health, Section of Nephrology, Federico II University, Naples, Italy are already available for our study.

The approval of the local Ethical Committee will be obtained before enrollment of patients, according to standard local procedures. Patients will sign an informed consent to allow the use of samples for research purposes.

Plasma will be obtained according to standard procedures during periodic follow-up admissions to the Hospital. Five ml of peripheral blood will be collected in EDTA and immediately processed, or stored at -80^0C.

Total RNA extraction preserving miRNA fraction, Small RNA-seq analysis in tissues, Small RNA-seq analysis in plasma and *Bioinformatic Analysis* were done as indicated previously (materials and methods of chapter 1).

Conclusive remarks

FD is one of the most common LSD. Also for this disease we have explored the potential of miRNAs as new tool for understanding of the diseases pathophysiology and as new potential biomarkers to follow disease diagnosis, progression and follow up of patients.

The NGS-based approach showed differentially expressed miRNAs in heart and kidney from the FD mouse. NGS screenings at additional time points, particularly in more advanced stages of disease,are in progress to better characterize the evolution of miRNA abnormalities in FD. As for PD, this analysis might result in the identification of circulating DE-miRNAs with statistical significance and in the identification of additional tissue-specific DE-miRNAs in target organs of the disease. To identify putative miRNA biomarkers in FD then we will implement our screening strategy on patients.

Chapter 3

Understanding the mechanisms underlying the pathophysiology of Pompe disease: inflammation and effect of glucocorticoids.

Introduction

Inflammation and muscle in PD

Some observations suggest that inflammation may play an important role in the pathophysiology of LSDs in general, including PD. Inflammation has been recently described in some LSDs, such as Multiple Sulfatase Deficiency or Niemann-Pick disease type C1 [Einat et al, 2010]. Nothing is known about the possible role of inflammation in PD muscle.

Strenuous muscle exertion or injuries typically initiate a rapid and sequential invasion of muscle by inflammatory cell populations that can persist for days to weeks, while muscle repair, regeneration, and growth occur. This relationship between inflammation and muscle repair or regeneration has suggested that they may be mechanistically related and provides the basis for the idea that muscle inflammation after injury is a functionally beneficial response. However, experimental observations have only recently begun to test that hypothesis and to distinguish between features of muscle inflammation that promote injury and those that promote growth or repair [James et al, 2005].

Macrophages play an essential role in the immune response and normal tissue development by producing proinflammatory mediators and by phagocytic clearance of pathogens and apoptotic cells [Lombardo et al, 2007; Bosca et al, 2005]. It has been described that macrophages could undergo different activation processes depending on the stimuli received.

- The classic activation, which can be induced by in vitro culture of macrophages with IFN-g and LPS (inducing TNF-a production), is associated with high microbicidal activity, proinflammatory cytokine, and reactive oxygen species production and cellular immunity;
- the innate activation, which is mediated in culture by ligation of receptors, such as TLRs, is associated with microbicidal activity and proinflammatory cytokine production;
- the alternative activation, which can be mimicked in vitro after culture with IL-4, IL-13, glucocorticoids, immune complexes, or IL-10, is associated with tissue repair, tumor progression, and humoral immunity [Gordon et al, 2005; Mantovani et al, 2005].

Pathways involved in the activation of inflammation

There are several pathways which may have an important (albeit poorly known) role in inflammation and muscle damage in PD.

Nuclear Factor Kappa B (NF-kB) is a major trascription factor espressed in wide variety of cells and modulating the cellular immune, inflammatory and proliferative responses [Karin, 1999].

Recently, the role of NF-kB in the skeletal muscle wasting process is gaining increasing attention, mainly because NF-kB is activated in response to several inflammatory molecules that cause muscle loss [Messina et al, 2011; Messina et al, 2006].

The inhibition of NF-kB activity by GCs is relevant for their anti-inflammatory action [Ana et al, 2007]. Moreover an involvement of NF-kB in myogenesis has been suggested because its activity was shown to be required by human and rat myoblasts to fuse into myotubes and to express muscle-specific proteins, such as myosin heavy chain and claveolin3 [Kaliman et al, 1999]. It has also been demonstrated that systemic administration of the NF-kB inhibitor curcumin stimutales muscle regeneration after traumatic injury, suggesting that modulation of NF-kB activity within muscle tissue could be beneficial for muscle repair [Thaloor et al, 1999].

The study of this pathway in PD skeletal muscle and heart could help in understanding of PD physiopathology and colud provide new therapeutic targets.

Effects of glucocorticoids

Pompe patients are caracterized by increased levels of muscular isoform of creatin-kinase (CK), as marker of muscular damage. Our unpublished experience suggests that when PD patients, occasionally and for intercurrent illnesses, are treated by steroid therapy, show a substantial reduction of CK levels. This reduction is temporary and ends when steroid therapy is discontinued.

Glucocorticoids (GCs), have a key role in maintaining muscle integrity. Many stress conditions are accompanied by skeletal muscle dysfunction and regeneration, which is essentially a recapitulation of the embryonic

development. However, regeneration usually occurs under conditions of hypothalamus-pituitary-adrenal gland axis activation and therefore increased GCs levels. Skeletal muscle is a prominent target for GCs in healt and disease [Schweicker et al, 2007; Menconi et al, 2007; Glass et al, 2010].

GCs are currently the only effective pharmacological treatment for Duchenne muscular dystrophy, where degeneration-regeneration cycle is a prominent feature, and they were even reported to enhance differentiation in skeletal muscle precursors from mdx mice [Passaquin et al 1993; Bach et al, 2010; Matthews et al, 2010; Ciciliot et al, 2010]. The benefical effect of steroid therapy in slowing the progression of DMD has been widely demonstrated in the literature [Mendell et al, 1989; Biggar et al, 2006]. A recent paper reports the ultrastructural changes following steroid therapy in dystrophic muscles. The presence of morphological changes following steroid therapy supports the beneficial therapeutic effects of steroids in muscle dystrophy. In this regard, further investigations are required to determine if these steroid-associated ultrastructural changes reflect underlying molecular changes. In particular steroid therapy in dystrophic muscle is associated with reduced numbers of dendritic cells and fibroblasts and increased numbers of satellite cells [Mahmoud et al, 2010]. Moreover the anti-infiammatory action of GCs result also from the inhibition of the activity of trascription factors as NF-kB by different mechanisms.

Based on these premises it would be interesting to investigate a possible role of GCs effect on muscular damage in PD.

Data on GCs signaling during human skeletal muscle regeneration, which is characterized by satellite cell activation, myoblast proliferation, fusion into myotubes and later by (re)innervation and maturation into fully developed muscle fibers [Chargè et al, 2004; Ciciliot et al, 2010], remain still incomplete.

Objectives

Other aim of the project is to investigate the presence and the role of inflammation in muscles of PD mice and patients and to identify possible target of innovative therapeutic strategy for PD. It would also be interesting to investigate a possible role of GCs effect on muscular damage in PD. Data on GCs signaling during human skeletal muscle regeneration remain still incomplete and the benefical effect of steroid therapy on muscle is a controversial topic.

Preliminary results

Our preliminary experiment to understand whether inflammation is present or not in PD muscles showed infiltrating macrophages among muscle fibers of PD mice.

The experiment was performed in muscle from PD mice at different ages (3 months and 9 months), that represented different stages of the disease progression. The presence of infiltrating macrophages was already detectable at 3 months, but was more appreciable at 9 months compared to control healty mouse muscle (as shown in FIGURE 10).

FIGURE 10

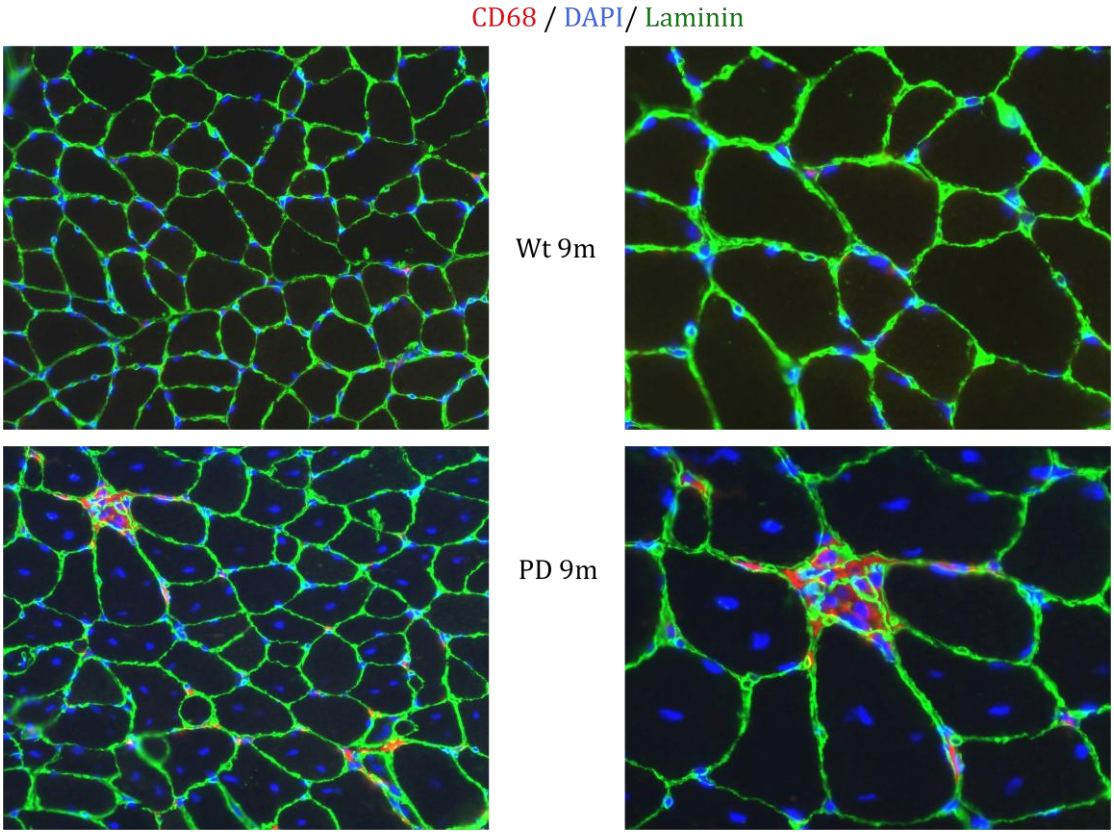

Muscle tissue (quadriceps) was stained with a macrophages specific marker (cd68) in red and with a basal lamina specific marker (laminin) in green.

Ongoing objective

Objective 1: To study the expression of different cytokines and additional markers of inflammation at different and more advantaged time points. This study in necessary to better characterize inflammation in PD, that is a field little knonw in this disease.

Objective 2: To study the effect of GC *in-vivo*. At this aim PD mice at different ages will be injected with selected GCs and then will be evaluate their effect at different time post injection.

Objective 3: correlation

Conclusive remarks

This part of the project is in a very preliminary phase. We have shown the presence of inflammation in PD mouse model muscle, a pathologic finding that has never been reported in earlier studies. This finding may be potentially

relevant for the identification of additional targets of therapy in PD and the development of multidisciplinary therapeutic strategies.

Chapter 4
Lysosomal enzymes assays in study of Wilson disease (collaboration)

“Wilson Disease Protein ATP7B Utilizes Lysosomal Exocytosis to Maintain Copper Homeostasis”

Introduction

Copper is an essential yet toxic metal and its overload causes Wilson disease, a disorder due to mutations in copper transporter ATP7B. To remove excess copper into the bile, ATP7B traffics toward canalicular area of hepatocytes. However, the trafficking
mechanisms of ATP7B remain elusive. Here, we show that, in response to elevated copper, ATP7B moves from the Golgi to lysosomes and imports metal into their lumen. ATP7B enables lysosomes to undergo exocytosis through the interaction with p62 subunit of dynactin that allows lysosome translocation toward the canalicular pole of hepatocytes.
Activation of lysosomal exocytosis stimulates copper clearance from the hepatocytes and rescues the most frequent Wilson-disease-causing ATP7B mutant to the appropriate functional site.

I have collaborated at this project since I have experience in the field of lysosomal enzymatic assays. Determination of b-Galattosidase and b-Hexosaminidase activities have been useful to understand the final findings of this study: they indicated that lysosomes serve as an important intermediate in ATP7B trafficking, whereas lysosomal exocytosis operates as an integral process in copper excretion and hence can be targeted for therapeutic approaches to combat Wilson disease.

CellPress

Developmental Cell
Article

Wilson Disease Protein ATP7B Utilizes Lysosomal Exocytosis to Maintain Copper Homeostasis

Elena V. Polishchuk,[1] Mafalda Concilli,[1] Simona Iacobacci,[1] Giancarlo Chesi,[1] Nunzia Pastore,[1,2] Pasquale Piccolo,[1] Simona Paladino,[3] Daniela Baldantoni,[4] Sven C.D. van IJzendoorn,[5] Jefferson Chan,[6] Christopher J. Chang,[6] Angela Amoresano,[7] Francesca Pane,[7] Piero Pucci,[7] Antonietta Tarallo,[1] Giancarlo Parenti,[1,8] Nicola Brunetti-Pierri,[1,8] Carmine Settembre,[1,2,8,9,10] Andrea Ballabio,[1,2,8,9] and Roman S. Polishchuk[1,*]

[1]Telethon Institute of Genetics and Medicine (TIGEM), Naples 80131, Italy
[2]Jan and Dan Duncan Neurological Research Institute, Houston, TX 77030, USA
[3]Department of Molecular Medicine and Medical Biotechnology, Federico II University, Naples 80125, Italy
[4]University of Salerno, Fisciano (SA) 84084, Italy
[5]Department of Cell Biology, University of Groningen, University Medical Center Groningen, Groningen 9713, the Netherlands
[6]Department of Chemistry and Molecular and Cell Biology and Howard Hughes Medical Institute, University of California, Berkeley, Berkeley, CA 94720, USA
[7]Department of Chemical Sciences, University of Naples Federico II, Napoli 80126, Italy
[8]Medical Genetics, Department of Translational and Medical Sciences, Federico II University, Naples 80125, Italy
[9]Department of Molecular and Human Genetics, Baylor College of Medicine, Houston, TX 77030, USA
[10]Dulbecco Telethon Institute, TIGEM, Naples 80131, Italy
*Correspondence: polish@tigem.it
http://dx.doi.org/10.1016/j.devcel.2014.04.033
This is an open access article under the CC BY license (http://creativecommons.org/licenses/by/3.0/).

SUMMARY

Copper is an essential yet toxic metal and its overload causes Wilson disease, a disorder due to mutations in copper transporter ATP7B. To remove excess copper into the bile, ATP7B traffics toward canalicular area of hepatocytes. However, the trafficking mechanisms of ATP7B remain elusive. Here, we show that, in response to elevated copper, ATP7B moves from the Golgi to lysosomes and imports metal into their lumen. ATP7B enables lysosomes to undergo exocytosis through the interaction with p62 subunit of dynactin that allows lysosome translocation toward the canalicular pole of hepatocytes. Activation of lysosomal exocytosis stimulates copper clearance from the hepatocytes and rescues the most frequent Wilson-disease-causing ATP7B mutant to the appropriate functional site. Our findings indicate that lysosomes serve as an important intermediate in ATP7B trafficking, whereas lysosomal exocytosis operates as an integral process in copper excretion and hence can be targeted for therapeutic approaches to combat Wilson disease.

INTRODUCTION

Copper is an indispensable micronutrient because a number of enzymes require it as a cofactor for fundamental metabolic processes such as respiration; free radical scavenging; pigmentation; and synthesis of collagen, elastin, and neurotransmitters (Lutsenko, 2010; Nevitt et al., 2012). However, due to its redox potential, copper can induce cellular toxicity. To avoid toxic accumulation of Cu, vertebrates developed a fine-tuned mechanism that allows excess Cu to be removed from the organism through the Cu-transporting ATPase ATP7B. ATP7B is a large multidomain protein with eight transmembrane helices, which form a channel that pumps Cu from the cytosol at the expense of ATP hydrolysis (Figure 1A). ATP7B is highly expressed in liver, where it normally resides in the trans-Golgi network (TGN) of hepatocytes and loads Cu on newly synthetized ceruloplasmin, the major Cu-carrying protein in the blood (Lutsenko, 2010). When intracellular Cu levels increase, ATP7B is thought to traffic toward the biliary surface of hepatocytes and associated "vesicles" involved in the excretion of Cu into bile. Mutations in the *ATP7B* gene frequently result in the failure of its protein product to traffic to the sites of Cu excretion. This defect causes toxic accumulation of Cu in the liver and, as a consequence, development of Wilson disease that is fatal if not treated in time (Gupta and Lutsenko, 2009).

Despite the fundamental role of ATP7B trafficking in Cu homeostasis, the intracellular itinerary of ATP7B transport remains poorly understood and controversial (La Fontaine and Mercer, 2007; Polishchuk and Lutsenko, 2013). First, in contrast to common view, several studies conducted in hepatic cells indicate that Cu does not alter the intracellular distribution of ATP7B (Harada et al., 2000, 2005). Second, the uncertainty in ATP7B trafficking concerns the identity of the peripheral vesicular structures, whose ability to receive ATP7B upon Cu overload was associated with a Cu excretion process (La Fontaine and Mercer, 2007; Polishchuk and Lutsenko, 2013). The majority of studies failed to demonstrate any significant overlap between ATP7B vesicles and common exo- or endocytic markers (Guo et al., 2005; La Fontaine et al., 2001), whereas few publications reported a fluorescent ATP7B fusion protein within the late endosome compartment (Harada et al., 2000, 2005). Therefore, the simple term "vesicles" is often applied to ATP7B-positive structures because lack of coherent data identifying their molecular composition and ultrastructure makes it problematic to classify them as specific exo- or endocytic organelles. Finally, the

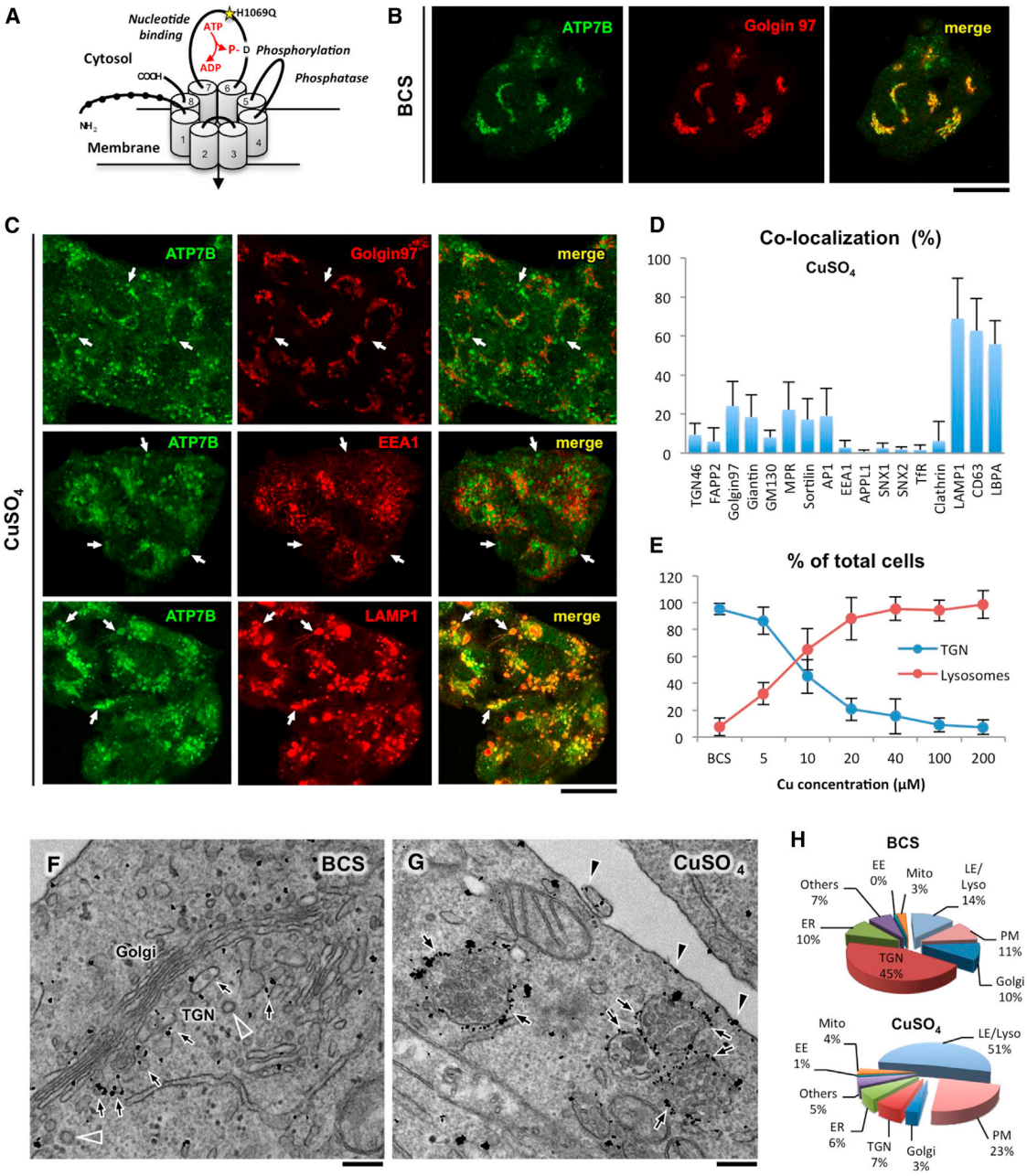

Figure 1. Increasing Cu Concentration Triggers ATP7B Trafficking from the TGN to LE/Lysosome Compartments

(A) Schematic structure of ATP7B. Black balls show N-terminal metal-binding domains. Numbers indicate transmembrane helices. The domains, which regulate ATPase activity, are indicated in italic with D residue for catalytic phosphorylation and with most frequent WD-causing mutation, H1069Q (yellow star).

(B) HepG2 cells were fixed after overnight exposure to 200 μM BCS and stained for endogenous ATP7B and golgin 97.

(C) BCS-treated cells were washed and incubated with 200 μM $CuSO_4$ for 2 hr. Confocal microscopy reveals endogenous ATP7B in vacuolar structures (arrows), which did not contain Golgin 97 or EEA1 but were decorated by LAMP1.

(D) Quantification shows ATP7B colocalization (mean ± SD; n = 50 cells) with lysosomal markers.

(E) Percentage (mean ± SD; n = 20 fields) of the cells with ATP7B in the TGN or in the lysosomes was calculated for treatments with BCS or with different concentration of $CuSO_4$ (as indicated along x axis).

(F and G) HepG2 cells were infected with adenovirus carrying ATP7B-GFP (adeno-ATP7B-GFP) and incubated with BCS. Then, the cells were fixed either directly (F) or after 2 hr incubation with $CuSO_4$ (G) and immunogold labeled to reveal ATP7B-GFP. Arrows indicate ATP7B signal over the TGN membranes in low Cu (F) or over the MVB/lysosome-like structures (G) in elevated Cu. Arrowheads show ATP7B at the cell surface in cells exposed to $CuSO_4$ (G).

(H) Pie plots exhibit percentage of ATP7B-associated gold particles in different compartments in cells treated with BCS or $CuSO_4$. EE, early endosome.

The scale bars represent 5 μm (B and C) or 250 nm (F and G).

question on whether or not ATP7B really reaches the canalicular surface of hepatocytes became the issue of ongoing debate (Hubbard and Braiterman, 2008).

As a consequence of above gaps in understanding of ATP7B trafficking, it is yet to be determined (1) which transport route is employed by ATP7B to reach "vesicles" and from where it emerges, (2) whether and how ATP7B gets delivered from "vesicles" to the canalicular surface of hepatocytes, and (3) how ATP7B trafficking is coordinated with Cu excretion from the cell.

Here, we show that an increase in Cu concentration induces direct ATP7B trafficking from the TGN to a subset of lysosomes, where ATP7B imports Cu for storage in the lysosome lumen and through the interaction with p62 subunit of dynactin complex enables lysosomes for polarized exocytosis at the canalicular surface of hepatocytes. Activation of lysosomal exocytosis stimulates both the delivery of ATP7B and its Wilson-disease-causing mutant to the canalicular membrane domains of hepatocytes and the release of excess Cu into the bile. Thus, our findings indicate ATP7B-containing lysosomes and lysosomal exocytosis as key components of Cu homeostasis.

RESULTS

Cu Induces ATP7B Redistribution from the TGN to Late-Endosome/Lysosome Compartments

We first investigated trafficking and localization of ATP7B in hepatoma HepG2 cells under different conditions varying in Cu levels. HepG2 cells express endogenous ATP7B and maintain key properties of normal hepatocytes, representing a reliable system to investigate trafficking of human ATP7B (Cater et al., 2006; Roelofsen et al., 2000). Figure 1B shows that Cu chelation with bathocuproine disulphonate (BCS) resulted in ATP7B accumulation in the Golgi region, where ATP7B colocalized with the TGN marker golgin-97. To stimulate ATP7B trafficking from the TGN, BCS-treated cells were washed and exposed to 200 μM $CuSO_4$ for 2 hr. This resulted in complete loss of the ATP7B from the TGN and its relocation to peripheral vesicular structures (Figure 1C, arrows). To determine whether these structures belong to an annotated exo- or endocytic compartment, we tested a battery of markers for overlap with the endogenous ATP7B. Confocal microscopy revealed significant colocalization between ATP7B and the late-endosome (LE)/lysosome markers LAMP1, CD63, and LBPA in the vesicular structures (Figures 1C and 1D and Figure S1A available online). In addition, we analyzed the distribution of the S340A mutant of ATP7B, which constantly resides in "vesicular" compartments (Hasan et al., 2012), and found its robust overlap with LAMP1 (Figure S1B). These observations suggest that ATP7B traffics from the TGN to the LE/lysosome compartment in response to elevated Cu. This process was extremely sensitive to Cu. Even relatively low (5–20 μM) Cu concentration induced ATP7B trafficking to LE/lysosomes (Figure 1E). Importantly, we also found LAMP1-, CD63-, and LBPA-positive organelles without ATP7B signal, indicating that only a subset (about 40%) of the LE/lysosomes received ATP7B from the TGN (Figure S1C).

To further verify LE/lysosomal targeting of ATP7B, we employed immuno-electron microscopy (EM) analysis of ATP7B-GFP that exhibited trafficking and localization similar to the endogenous ATP7B (Figure S1D). In response to Cu, ATP7B-GFP moved from the tubular-vesicular TGN membranes (Figure 1F, arrows) to large multivesicular body (MVB)-like structures (Figure 1G, arrows; see also morphometry in Figure 1H), which contained numerous intraluminal vesicles (ILVs) and/or heterogeneous electron dense material (Figures 2A and 2B). These ultrastructural features allowed us to assign ATP7B-containing organelles to the LE/lysosome compartment (Saftig and Klumperman, 2009). Indeed, a double immunogold labeling revealed ATP7B-positive MVBs to contain LAMP1 (Figure 2B). Finally, we verified whether ATP7B is also transported to LE/lysosomal structures in vivo. Thin sections of mice liver revealed ATP7B-GFP (expressed via adenoviral vector) in MVB-like structures decorated by LAMP1 (Figure 2C) and similar to those observed in HepG2 cells. Therefore, ATP7B "vesicles" in the HepG2 line and in mouse hepatocytes can be defined as LE/lysosomes from both molecular and ultrastructural standpoints (for convenience, we will call them "lysosomes" through the rest of the manuscript).

Lysosomal localization of ATP7B prompted us to investigate whether the protein is directed to lysosomes for degradation that requires sorting into ILVs located in the lumen of lysosomes (Saftig and Klumperman, 2009). We found that only a small fraction of ATP7B was associated with ILVs and lysosome lumen (Figures 2A–2E), even when compared to LAMP1 (Figures 2A and 2E). Correspondingly, ATP7B levels remained unaffected when lysosome degradation was inhibited with bafilomycin A (Figure S2), indicating that ATP7B is targeted to lysosomes to perform a specific function at their limiting membranes, but not to be degraded.

ATP7B Is Transported to the Lysosomal Compartment through a Direct Route that Emerges from the TGN

In response to Cu, ATP7B may travel via two possible routes: (1) it may first be delivered from the TGN to the cell surface and then be endocytosed to the lysosomes (indirect pathway) or (2) ATP7B might be conveyed from the TGN directly to the lysosomal compartments (direct pathway). To distinguish between these two possibilities, we treated HepG2 cells with tannic acid (TA), which blocks both the exo- and endocytic events at the level of the plasma membrane (Polishchuk et al., 2004). This treatment would prevent ATP7B trafficking to the lysosomes through the indirect pathway but would not impact the direct route. As a control, HepG2 cells were infected with the vesicular stomatitis virus (VSV) to express a thermosensitive t-45Os version of VSV glycoprotein (VSVG), a bona fide exocytic marker (Polishchuk et al., 2003). The cells were incubated at 20°C with BCS to accumulate both VSVG and ATP7B within the Golgi (Figure 2F). Cells were then shifted to 32°C in the presence of $CuSO_4$ to activate both VSVG and ATP7B export from the TGN. In the absence of TA, VSVG was delivered from the TGN to the cell surface, whereas TA treatment caused VSVG arrest within TGN-derived transport carriers, which were docked at the plasma membrane (PM) but unable to fuse with acceptor membrane (Figure 2F). In contrast, accumulation of ATP7B within such post-Golgi VSVG-positive carries did not occur. Instead, most of ATP7B appeared within larger lysosome-like structures both in control and TA-treated cells (Figure 2F), indicating that ATP7B traffics directly from the TGN to lysosomes in response to an increase in Cu concentration.

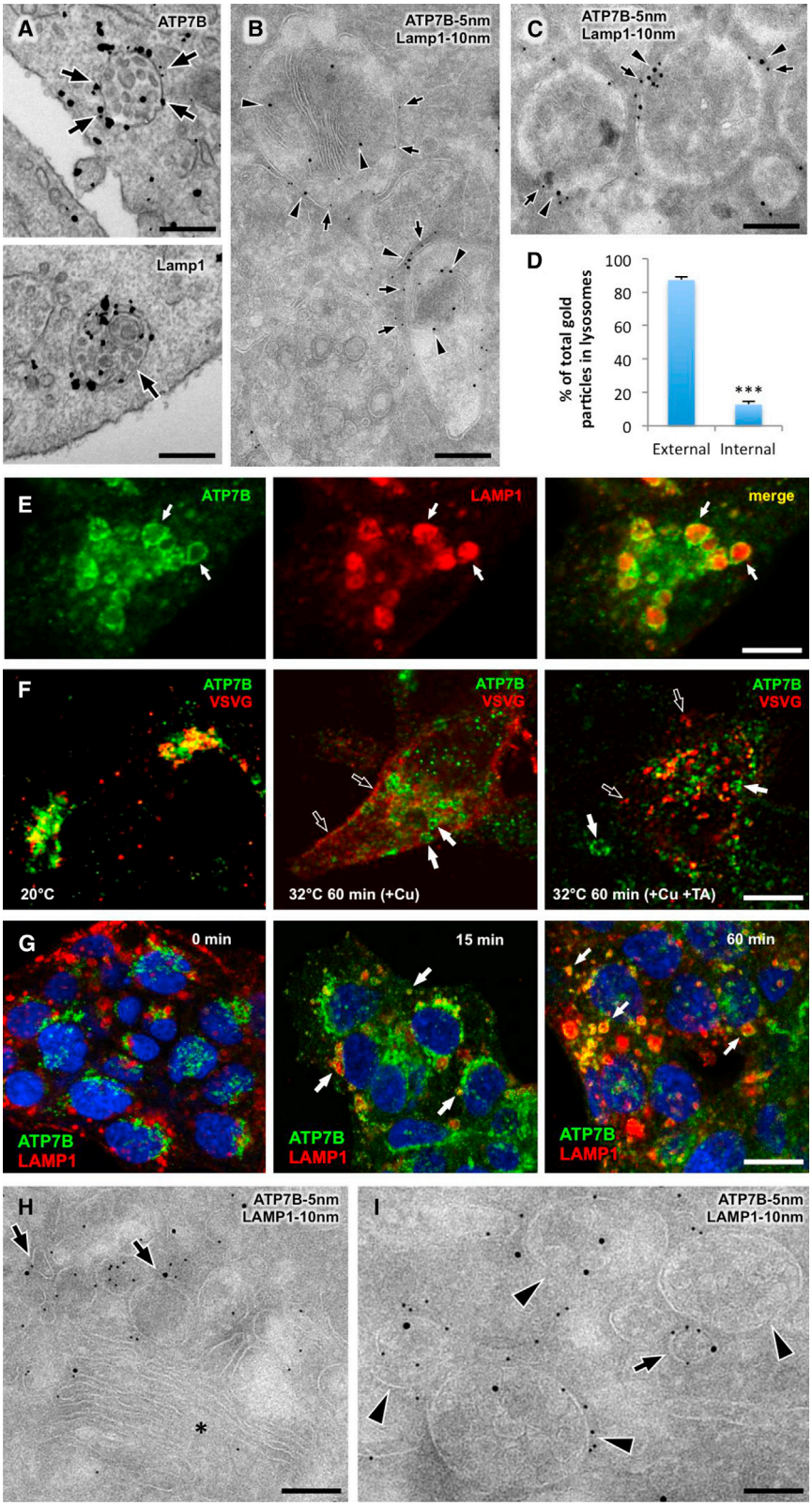

Figure 2. Lysosomes Retain ATP7B at Their Limiting Membranes and Receive ATP7B from the TGN through a Direct Route

(A) $CuSO_4$-treated HepG2 cells were immunogold labeled to reveal either ATP7B-GFP or LAMP1. Arrows in top panel indicate ATP7B distribution along limiting membrane of the MVBs, whereas some LAMP1 labeling can be seen at the internal membranes of lysosomes (arrow in bottom panel).

(B) $CuSO_4$-treated HepG2 cells were processed for cryo-immuno-EM. Arrows and arrowheads indicate ATP7B-GFP and LAMP1, respectively, within the same lysosome-like structures.

(C) Liver tissue from mice, which was injected with adeno-ATP7B-GFP and treated with $CuSO_4$, was labeled for ATP7B-GFP and LAMP1. ATP7B-GFP (arrows) and LAMP1 (arrowheads) were detected together within lysosome-like structures.

(D) Quantification of the percentage of gold particles in lysosomes (mean ± SD; n = 100 structures) shows most of ATP7B to reside at the external membrane.

(E) $CuSO_4$-treated HepG2 cells exhibit endogenous ATP7B as circles (arrows) at the surface of LAMP1-positive structures.

(F) HepG2 cells were infected with VSV (see Experimental Procedures) and fixed directly after 20°C block (left panel) or incubated at 32°C with $CuSO_4$ for 60 min with (right panel) or without (midpanel) tannic acid (TA). Empty arrows indicate VSVG at the cell surface (midpanel) and post-Golgi carriers (right panel), whereas filled arrows indicate lysosome-like ATP7B structures.

(G) HepG2 cells were fixed directly after incubation with BCS or exposed to $CuSO_4$ for either 15 min or 60 min and stained for endogenous ATP7B and LAMP1. Arrows indicate ATP7B/LAMP1-positive structures.

(H and I) HepG2 cells expressing ATP7B-GFP were incubated with BCS and fixed directly (H) or 15 min after incubation with $CuSO_4$ (I) and labeled for ATP7B-GFP and LAMP1. ATP7B and LAMP1 were detected in some TGN domains (H, arrows) of the Golgi stack (H, asterisk). Arrow in (I) indicates ATP7B/LAMP1 post-Golgi carrier near the ATP7B/LAMP1-positive MVBs (arrowheads).

The scale bars represent 250 nm (A), 150 nm (B, C, H, and I), 3.5 μm (E and F), and 7 μm (G).

To further verify this conclusion, we performed a time course analysis of ATP7B release from the TGN. As soon as 15 min after Cu addition, the ATP7B signal was detected in LAMP1-positive structures (Figure 2G, arrows). Such a fast rate of ATP7B trafficking argues against the indirect pathway because the uptake from the PM to lysosomes alone usually takes at least 30 min (Saftig and Klumperman, 2009). In addition, no ATP7B was observed at the surface of hepatocytes at that time point. Later (30 and 60 min after $CuSO_4$ addition), the number of ATP7B-containing lysosomes progressively increased, whereas the Golgi area gradually lost the ATP7B signal (Figure 2G), supporting the direct transfer of ATP7B from the TGN to the lysosomal compartments.

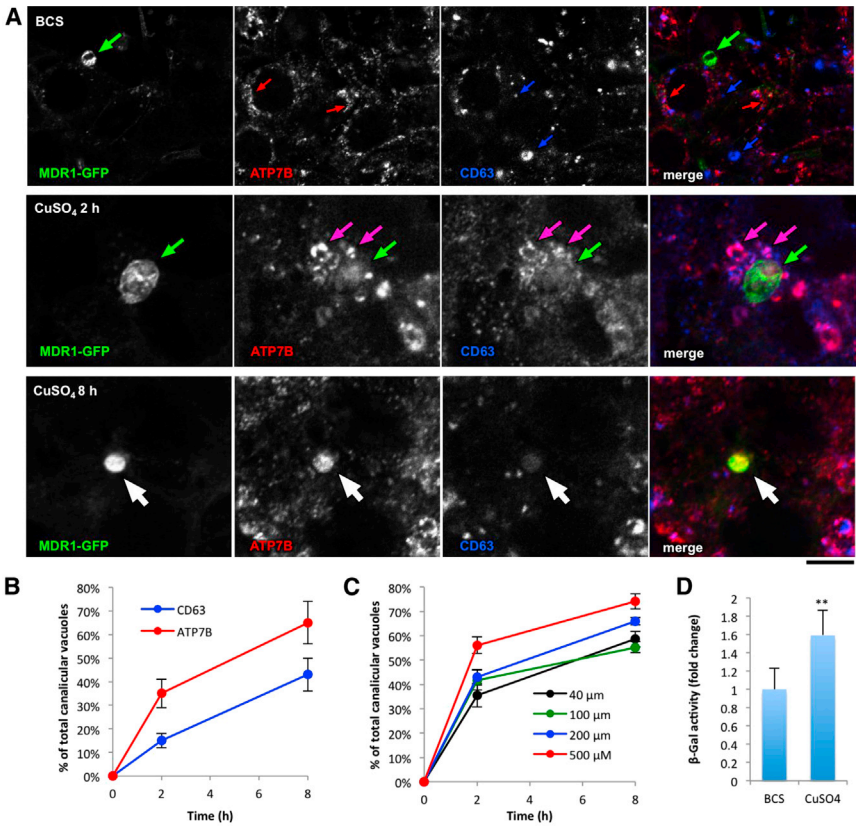

Figure 3. ATP7B Delivery to the Canalicular Domain of Polarized HepG2 Cells Requires a Lysosome Intermediate

(A) Polarized HepG2-MDR1 cells were fixed directly after incubation with BCS or after additional treatment with $CuSO_4$ for either 2 hr or 8 hr. After incubation with BCS, ATP7B was detected mainly within Golgi membranes (red arrows) but neither in CD63-positive lysosomes (blue arrows) nor in canalicular vacuoles (green arrows). Exposure to $CuSO_4$ (2 hr) triggered ATP7B relocation to CD63-positive structures (pink arrows), which were frequently clustered around apical cysts (green arrows). White arrows in the lower row show canalicular vacuole, which received both ATP7B and CD63 after 8 hr incubation with $CuSO_4$.

(B) The percentage (mean ± SD; n = 20 fields) of ATP7B-positive or CD63-positive canalicular vacuoles increased in HepG2 cells over the time of incubation with $CuSO_4$.

(C) The cells were treated like in (A) with the exception that different $CuSO_4$ concentrations were utilized. The percentage (mean ± SD; n = 20 fields) of ATP7B-positive canalicular vacuoles was calculated and plotted as a function of time.

(D) Polarized HepG2-MDR1 cells were with BCS overnight or with $CuSO_4$ for only 8 hr. The activity of β-Gal (mean ± SD; n = 3 experiments) in the canalicular cysts exhibits increase upon Cu stimulation.

The scale bar represents 6.5 μm (A).

We next investigated which Golgi-to-lysosome pathway is utilized by ATP7B. A large cohort of lysosomal proteins is carried from the TGN to endolysosomal compartments through transport events driven by clathrin and its adaptors, AP-1 and GGA (Saftig and Klumperman, 2009), whereas other lysosome residents (such as LAMP1 and MHC-II) take a clathrin-independent TGN-to-lysosome route (Pols et al., 2013; Saftig and Klumperman, 2009). We found that ATP7B did not associate with clathrin-coated profiles (Figure 1F, arrowheads) in the TGN area under neither low nor high Cu conditions. This is consistent with recent observations that neither AP-1 nor GGA suppression affects ATP7B export from the Golgi (Hirst et al., 2012). Further examination revealed ATP7B enrichment over the smooth TGN membrane domains (arrows in Figures 1F and 2H), which often contained LAMP1 (Figure 2H, arrows). Shortly after Cu stimulation, ATP7B was detected within 70–200 nm round or elongated membrane carriers, which occasionally exhibited internal membranes (Figure 2I, arrow) and therefore were similar to structures operating in direct Golgi-to-lysosome transport of LAMP1 (Pols et al., 2013). Indeed, these ATP7B carriers also frequently contained LAMP1 and were docked to the MVB-like structures (Figure 2I), indicating that ATP7B and LAMP1 may use the same pathway to travel from the TGN to lysosomal compartments.

ATP7B Is Delivered from Lysosomes to Canalicular PM in Polarized Hepatocytes

ATP7B trafficking to lysosomes in response to Cu was unexpected and raised a question about the mechanism through which the lysosomes mediate Cu excretion from hepatocytes. One possibility would be that Cu efflux occurs through lysosomal exocytosis, a mechanism by which lysosomes fuse with the PM and secrete their content to the outside the cell (Andrews, 2000).

To examine whether ATP7B-containing lysosomes undergo apical exocytosis, we grew HepG2 cells under conditions that allowed for their polarization (Slimane et al., 2003). Upon polarization, neighboring hepatocytes form an apical (or biliary) cyst (vacuole) enriched in specific apical markers such as biliary salt transporters MDR1, MRP2, etc. (Slimane et al., 2003). Polarized HepG2 cells stably expressing canalicular marker MDR1-GFP (Slimane et al., 2003) were incubated with BCS to trap ATP7B within the Golgi and then exposed to 200 μM $CuSO_4$ to follow the fate of ATP7B. In low Cu, ATP7B was mostly detected in the Golgi area (Figure 3A). Two hours after Cu stimulation, ATP7B exhibited a significant overlap with CD63 in lysosomes, which were frequently clustered around the biliary surface of the cells (Figure 3A). Notably, over 40% of apical cysts already exhibited ATP7B signal at this time point (Figure 3B). When incubation with $CuSO_4$ was extended to 8 hr, the ATP7B labeling became more evident in canalicular cysts with 60% of them being ATP7B positive (Figures 3A and 3B). We also found that the redistribution of ATP7B to the canalicular domain of the cells occurred even upon moderate Cu increase (20–40 μM) and correlated with concentration of Cu and the duration of $CuSO_4$ treatment (Figure 3C). A lower concentration of Cu (10 μM) was unable to induce ATP7B delivery to the canalicular membrane of HepG2 cells, although it still allowed for efficient ATP7B redistribution from the TGN to lysosomes (see Figure 1E).

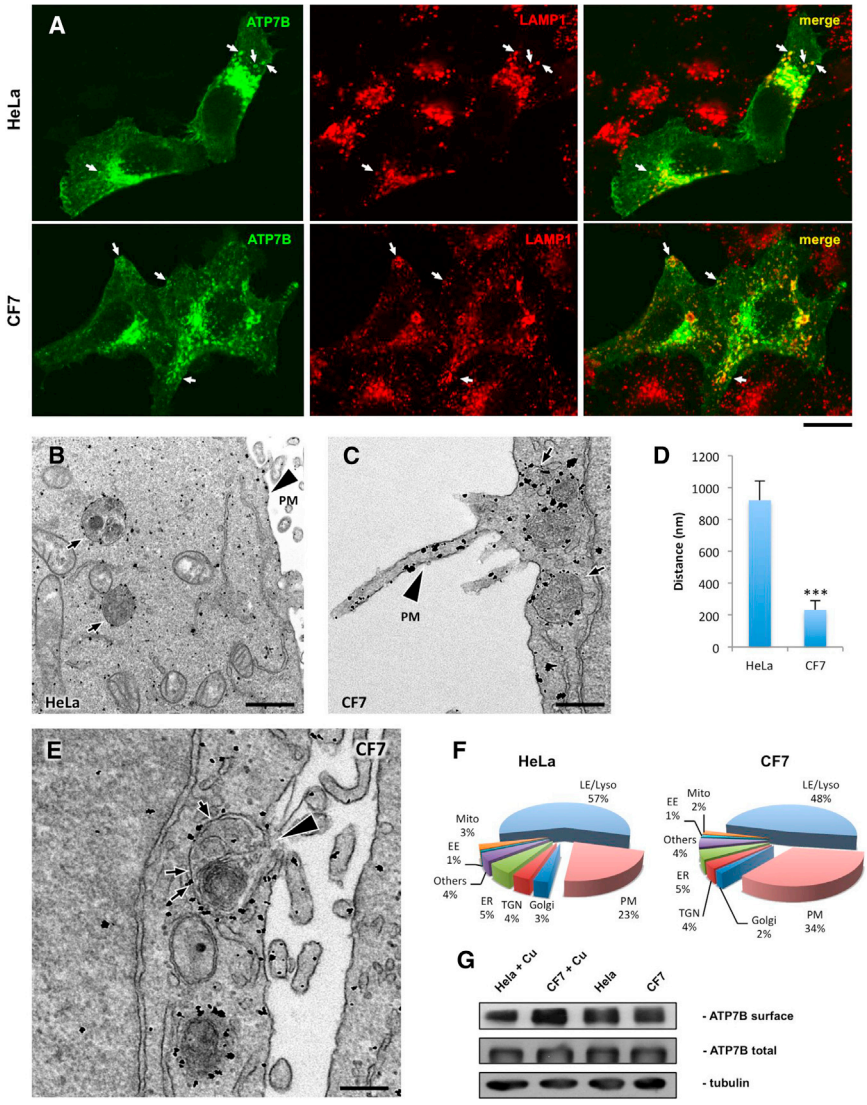

Figure 4. Activation of Lysosomal Exocytosis Stimulates Delivery of ATP7B to the Plasma Membrane

(A) HeLa or CF7 cells were infected with adeno-ATP7B-GFP, incubated with $CuSO_4$ for 2 hr, fixed, and stained for LAMP1. Arrows indicate ATP7B in lysosomes.

(B and C) HeLa (B) or CF7 cells (C) were treated as in (A) and processed for immunogold EM to reveal ATP7B-GFP distribution. In both cell types, elevated Cu triggered ATP7B delivery to the lysosome-like structures (B and C, arrows) and plasma membrane (B and C, arrowhead).

(D) Morphometry revealed reduction of the distance (mean ± SD; n = 100 lysosomes) between lysosomes and PM in CF7 cells.

(E) Arrowhead indicates the site of fusion between ATP7B-positive lysosome (arrows) and PM in CF7 cell.

(F) Pie plots exhibit percentage of ATP7B-associated gold particles in different compartments of HeLa and CF7 cells.

(G) HeLa and CF7 cells were infected with adeno-ATP7B-GFP and then prepared for surface biotinylation directly or 2 hr after stimulation with 200 μM $CuSO_4$. Western blot revealed higher amount of ATP7B at the surface of CF7 cells upon Cu increase.

The scale bars represent 3.8 μm (A), 280 nm (B), 240 nm (C), and 220 nm (E).

Interestingly, we also detected CD63 together with ATP7B in the apical vacuoles upon Cu stimulation (Figures 3A and 3B). This suggests that ATP7B and CD63 were delivered together to the apical cysts of hepatocytes, likely through the induction of lysosomal exocytosis in response to Cu stimulation. Indeed, ATP7B delivery to the canalicular area of hepatocytes coincided with an increase in activity of lysosomal enzyme β-galactosidase (β-Gal) in biliary cysts upon Cu stimulation (Figure 3D).

Thus, apical lysosomal exocytosis may serve as a main route for Cu excretion in hepatocytes because it allows for (1) release of Cu from the ATP7B-positive lysosomal stores and (2) delivery of ATP7B to the canalicular domain.

Modulation of Lysosomal Exocytosis Affects ATP7B Delivery to the PM

Given that lysosomal exocytosis seems to be involved in the delivery of ATP7B to the cell surface, we decided to verify whether modulation of this process impacts ATP7B trafficking to the PM. To this end, we first used the CF7 HeLa cells that stably overexpress transcription factor EB (TFEB), a potent activator of lysosomal exocytosis (Medina et al., 2011). Stimulation with $CuSO_4$ induced ATP7B redistribution from the Golgi to lysosomes and PM in both CF7 and parental HeLa cells (Figure 4A). CF7 cells exhibited ATP7B in numerous LAMP1-positive lysosomes positioned close to the peripheral regions of the cell membrane (Figure 4A). Such LAMP1-positive structures constitute a pool of peripheral lysosomes that actively undergo exocytosis (Medina et al., 2011). Indeed, EM revealed ATP7B in lysosome-like structures that were located significantly closer to the PM in CF7 cells than in control HeLa cells (Figures 4B and 4C, arrows, and 4D). Importantly, ATP7B-positive lysosomes were frequently seen to fuse directly with the PM in CF7 cells (Figure 4E), resulting in increase in the amount of ATP7B compared to the parental HeLa line (Figure 4F), as also confirmed by surface biotinylation (Figure 4G). Taken together, these observations suggest that TFEB-mediated activation of lysosomal exocytosis stimulates ATP7B delivery to the cell surface under high Cu conditions.

To test whether this is also the case in a liver-relevant cell system, polarized MDR1-GFP HepG2 cells were infected with a helper-dependent adenovirus carrying TFEB DNA (HDAd-TFEB) (Figures 5A–5D), which resulted in an increase in TFEB expression (Figure 5C). TFEB- and mock-infected cells were then exposed to $CuSO_4$, and the ATP7B signal in MDR1-GFP-positive biliary cysts was analyzed. We found that

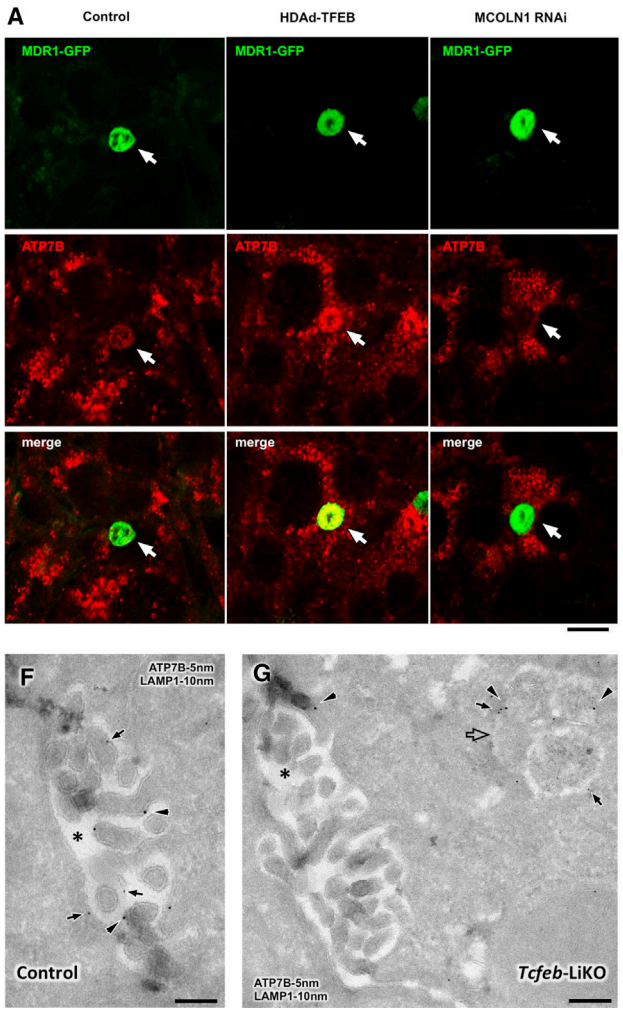

Figure 5. Modulation of Lysosomal Exocytosis Impacts ATP7B Delivery to the Canalicular Domains of Hepatic Cells In Vitro and In Vivo

(A) Polarized HepG2-MDR1 cells were infected with HDAd-TFEB (middle column) or incubated with MCOLN1-specific small interfering RNAs (siRNAs) (right column) and exposed to 200 μM $CuSO_4$ for 8 hr. Immunofluorescent labeling of endogenous ATP7B revealed increase in its amount in the area of canalicular vacuoles (arrows in the midcolumn) in the cells infected with HDAd-TFEB and decrease in the canalicular area (arrows in the right column) of MCOLN1-silenced cells.

(B) Quantification shows ATP7B-associated fluorescence in the MDR1-positive canalicular vacuoles (mean ± SD; n = 50 canalicular vacuoles).

(C) qRT-PCR indicated increase in TFEB mRNA levels in the cells infected with virus containing TFEB DNA.

(D) Western blot revealed that total amounts of endogenous ATP7B remained similar in control and TFEB-overexpressing cells.

(E) qRT-PCR shows decrease in MCOLN1 mRNA levels in MCOLN1-silenced cells.

(F and G) Liver tissue from the control and *Tcfeb*-LiKO mice injected with adeno-ATP7B-GFP were prepared for cryo-immuno-EM, which revealed ATP7B (F, arrows) and LAMP1 (F, arrowheads) in the canalicular region (F, asterisk) in control mice. LAMP1 (G, arrowheads) and ATP7B (G, arrows) exhibited poor signal at the canalicular membrane (G, asterisk) in *Tcfeb*-LiKO mice but were detected in neighbor lysosome (G, open arrow).

(H) ATP7B and LAMP1 labeling densities were calculated in canalicular domains (mean ± SD; n = 50 canalicular areas) and in lysosomes (mean ± SD; n = 50 lysosomes).

The scale bars represent 3.5 μm (A), 240 nm (F), and 270 nm (G).

overexpression of TFEB resulted in a higher amount of ATP7B delivered to the apical domain of HepG2 cells (Figures 5A and 5B), whereas the total quantity of ATP7B remained the same (Figure 5D).

In a parallel series of experiments, we inhibited lysosomal exocytosis by suppressing mucolipin-1 (MCOLN1) using RNAi. MCOLN1 is a Ca^{2+} channel, which promotes lysosome fusion with PM (Medina et al., 2011). Reduction of MCOLN1 expression in HepG2 cells (Figure 5E) resulted in a significant decrease in ATP7B delivery to biliary surface (Figures 5A and B). Given that Ca^{2+} is required for lysosomal exocytosis (Andrews, 2000), we used the Ca^{2+} chelator BAPTA as another tool to inhibit lysosomal exocytosis and observed reduction in ATP7B trafficking to the canalicular domain in BAPTA-treated cells (not shown).

Finally, we employed a mice model with a liver-specific knockout of *TFEB* (*Tcfeb*-LiKO mice) (Settembre et al., 2013) to evaluate whether inhibition of TFEB-mediated lysosomal exocytosis affects delivery of ATP7B to the canalicular sites of hepatocytes in vivo. To this end, control and *Tcfeb*-LiKO mice were given Cu in their drinking water as described (Gross et al., 1989). The mice were sacrificed 4 hr after stimulation with Cu and their livers processed for analysis. EM revealed specific ATP7B and LAMP1 signals in canalicular area of hepatocytes in the liver of control mice (Figure 5F), indicating efficient delivery of both proteins from the lysosomes upon Cu overload. The presence of ATP7B and LAMP1 at the canalicular membrane of hepatocytes correlated with increased activity of β-Gal and β-hexosaminidase (β-Hex) in the bile (Figure S3A). This suggests that Cu stimulates lysosomal exocytosis at the biliary surface of hepatocytes and thus facilitates ATP7B delivery from lysosomal structures to the canalicular membrane.

In contrast, *TFEB* deletion in the liver of *Tcfeb*-LiKO mice resulted in significant reduction of both ATP7B and LAMP1 labeling at the biliary membrane of hepatocytes (Figures 5G and 5H). We reasoned that the decrease of ATP7B at the canalicular domains in *Tcfeb*-LiKO mice liver was due to the suppression of lysosomal exocytosis. We found that ATP7B/LAMP1-positive lysosomes can be detected near canaliculi (Figure 5G) in *Tcfeb*-LiKO mice and that ATP7B/LAMP1 labeling densities in such lysosomes were similar to those in control animals (Figure 5H). However, deletion of *Tcfeb* did not allow ATP7B lysosomes to fuse with apical membrane of hepatocytes and therefore to convey ATP7B to the canalicular surface. This correlated with a significant reduction of β-Hex and β-Gal activities in the bile of *Tcfeb*-LiKO mice despite Cu stimulation (Figure S3B).

Thus, taken together, both in vitro and in vivo observations support the involvement of lysosomal exocytosis in targeting ATP7B to the biliary surface domain in hepatic cells.

Activation of Lysosomal Exocytosis Increases Copper Excretion from the Cells

To further test the impact of lysosomal exocytosis on Cu homeostasis, we investigated whether this process is involved in the regulation of Cu efflux from liver cells. Coppersensor 3 (CS3) was employed to analyze intracellular levels of exchangeable Cu (Dodani et al., 2011). Variations of intracellular Cu levels observed in the control experiments with CS3 (Figures 6A and 6B) were confirmed by spectroscopy (Figure 6C).

Then, we investigated subcellular distribution of CS3 in cells expressing ATP7B-GFP. HepG2 cells treated with BCS exhibited low CS3 signal in the cytoplasm, whereas ATP7B-GFP was mainly detected in the Golgi area (Figure 6D). Shortly (15 min) after exposing cells to Cu, ATP7B appeared in the lysosomes where increased CS3 signal was detected (Figure 6D). Longer incubation with $CuSO_4$ (up to 2 hr) induced a complete redistribution of ATP7B to the lysosomes (Figure 6D), where CS3 fluorescence further concentrated, indicating that ATP7B lysosomes could be used for temporary Cu storage/sequestration.

Next, we reasoned that activation of lysosomal exocytosis should allow reduction of intracellular Cu due to release of the metal from the lysosome into canalicular vacuoles. To test this, we used polarized HepG2 cells, which were infected with HDAd-TFEB to activate lysosomal exocytosis, exposed to $CuSO_4$, and labeled with CS3. Confocal microscopy revealed the CS3 signal to be higher in biliary cysts of TFEB-overexpressing cells than in those of control cells (Figures 6E–6G). Meanwhile, CS3 fluorescence decreased in the cytoplasm of TFEB-infected cells (Figure 6E). Elevation of Cu levels in the apical vacuoles of TFEB-overexpressing HepG2 cells was confirmed by inductively coupled plasma mass spectrometry (ICP-MS) (Figure 6H), indicating that stimulation of lysosomal exocytosis helps to excrete Cu from hepatocytes into biliary areas.

ATP7B Silencing Inhibits Apical Lysosomal Exocytosis, Cu Excretion, and Polarization of Hepatic Cells

We then determined whether ATP7B is required for lysosome exocytosis at the apical surface of hepatic cells. To this end, we silenced ATP7B expression in polarized HepG2 cells (Figures 7A and 7B) and found that, in contrast to control cells, ATP7B-deficient cells exhibited no CD63 within canalicular domains (Figure 7C, arrows). This finding suggests that ATP7B presence at the lysosomes might define their ability to undergo apical exocytosis. Interestingly, ATP7B ablation also affected polarization of HepG2 cells, as we detected a reduction in the number of hepatocytes making MDR1-positive canalicular cysts (Figures S4A, arrows, and S4B) and a mistargeting of MDR1 to the basolateral surface in silenced cells (Figures 7C, arrowheads, and S4A).

We also investigated the intracellular distribution of Cu in ATP7B-deficient cells. We detected CS3 fluorescence within the LAMP1-GFP-positive structures of control cells, whereas in ATP7B-silenced cells, CS3 was hardly visible in LAMP1-GFP spots (Figure 7D, arrows), indicating that lysosomes did not receive Cu in the absence of ATP7B. Finally, we also found that CS3 fluorescence in the canalicular area of ATP7B-deficient HepG2 cells was lower than in control hepatocytes (Figure 7E, arrows), whereas intracellular CS3 signal increased (Figures 7E and 7F). Elevated intracellular Cu levels in ATP7B-silenced HepG2 cells were also confirmed by ICP-MS (Figure 7G).

Taken together, these results indicate that ATP7B is involved (1) in Cu import into lysosomes and (2) in apical exocytosis of such lysosomes that allows elimination of excess Cu from the cells and supports hepatocyte polarity.

Cu-Dependent Interaction with p62 Dynactin Subunit Defines ATP7B Targeting to the Canalicular Surface of Hepatic Cells

To understand the molecular mechanism through which ATP7B targets lysosomes to the apical surface of hepatocytes, we analyzed the publications on Cu-dependent protein interactions of ATP7B. From this information, we found the interaction between ATP7B and the p62 subunit of dynactin (DNCT4) to be particularly attractive from the trafficking standpoint (Lim et al., 2006). Given that the minus ends of the microtubules are oriented toward the canalicular domain of hepatocytes (Cohen et al., 2004), the binding to p62 may allow ATP7B-containing membranes to anchor the dynein motor and, therefore, be translocated to the biliary surface.

To test this hypothesis, we first immunoprecipitated endogenous p62 from either BCS- or $CuSO_4$-treated HepG2 cells and found significantly higher amounts of ATP7B in pull-downs from the cells kept in high Cu (Figure 7H). Cu-dependent association of ATP7B with p62 was confirmed further using proximity ligation assay (PLA) (D'Agostino et al., 2013). Figure 7I shows a clear PLA signal, indicating close association between ATP7B and p62 in cells that were exposed to $CuSO_4$. Such PLA signal was lacking in BCS-treated cells (Figure 7I), suggesting that the effective interaction of ATP7B with p62 occurs only when the intracellular Cu increases. We then analyzed the impact of p62 silencing (Figure 7J) on Cu-dependent trafficking of ATP7B. We found that p62 depletion did not affect ATP7B transport from the Golgi to lysosomes upon increase in Cu concentration (Figure S4C). However, further clustering of ATP7B-contaning lysosomes around the apical cyst and delivery of ATP7B to the canalicular surface were seriously compromised in p62-deficient HepG2 cells (Figure 7K, arrows). To further evaluate the impact of p62-ATP7B interaction on the lysosomal exocytosis, we depleted p62 or ATP7B and measured the activity of lysosomal enzyme β-Gal within canalicular cysts of polarized HepG2 cells stimulated with $CuSO_4$. Both ATP7B-silenced and p62-silenced cells exhibited significant reduction of enzyme activities within the canalicular vacuoles (Figure 7L).

Notably, as it occurred in ATP7B-depleted cells, ablation of p62 resulted in partial loss of polarity of HepG2 cells and partial missorting of MDR1 from canalicular cysts (Figures 7K, arrowheads, S4D, and S4E). In contrast, the distribution of basolateral markers such as E-cadherin and Na/K-ATPase remained intact (Figure S4B) in silenced cells.

Taken together, these findings suggest (1) that the Cu-dependent interaction between ATP7B and p62 is required for apical exocytosis of ATP7B-positive lysosomes at the canalicular surface of hepatocytes and (2) that this process contributes to the polarization of HepG2 cells.

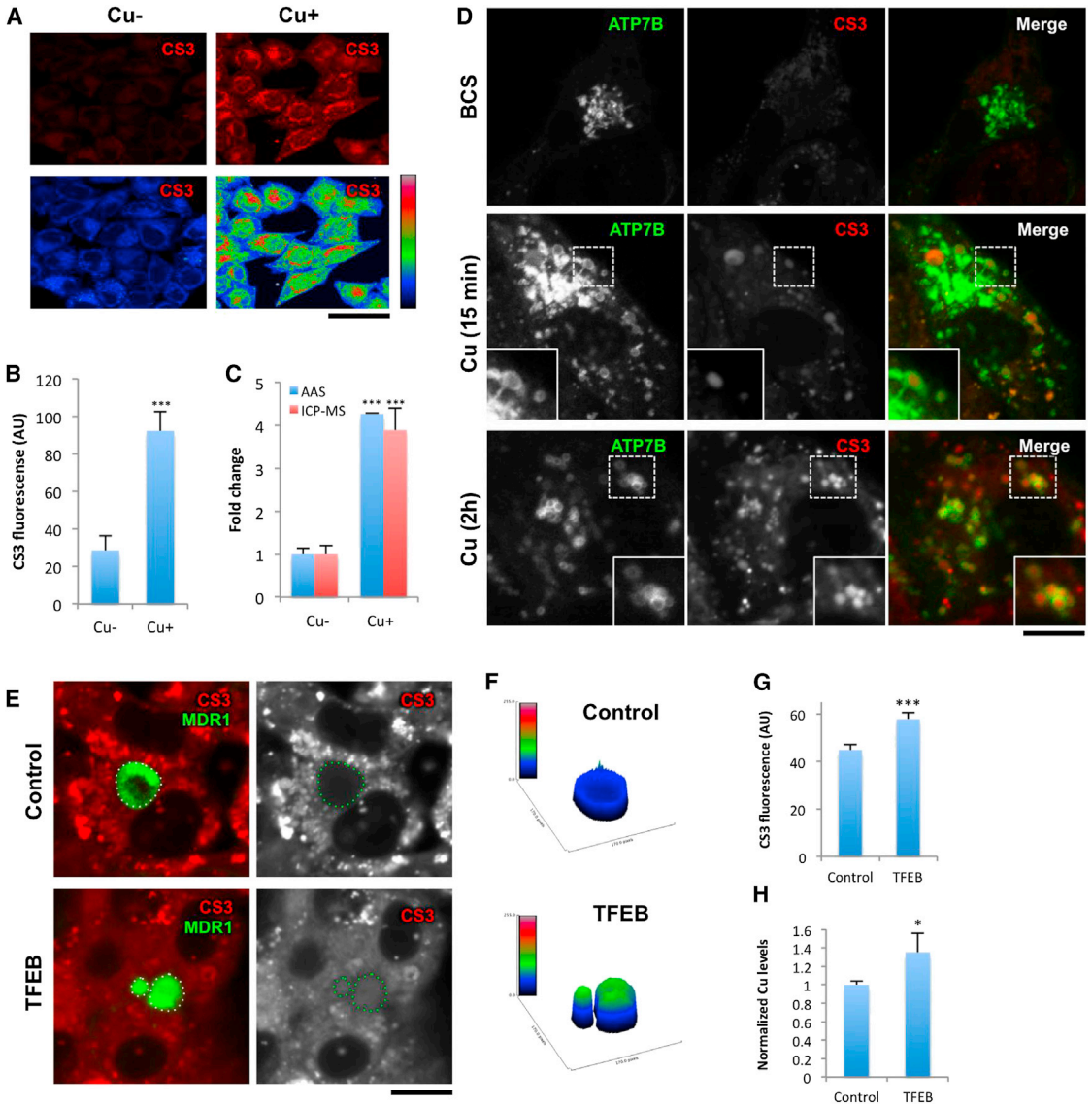

Figure 6. Activation of Lysosomal Exocytosis Stimulates Cu Excretion from HepG2 Cells

(A) HepG2 cells were incubated with either 200 μM BCS or 200 μM $CuSO_4$ for 2 hr loaded with CS3 for 15 min before visualization at the confocal microscope. Cu-associated CS3 signal was low in BCS-treated cells but significantly increased in Cu-loaded cells (see false color images of CS3 intensity in lower row).

(B) Quantification of the CS3 fluorescent intensity (mean ± SD; n = 15 fields) indicated its increase in $CuSO_4$-treated cells.

(C) Cells were treated like in (A) and prepared for atomic adsorption spectroscopy (AAS) or inductively coupled plasma mass spectrometry (ICP-MS), which revealed an increase in intracellular Cu concentration (mean ± SD; n = 4 experiments) in $CuSO_4$-treated cells.

(D) HepG2 cells were infected with adeno-ATP7B-GFP, exposed to BCS, and observed in confocal microscope either directly or after 15 min or 2 hr incubation with $CuSO_4$. Insets show CS3 fluorescence within circular ATP7B lysosomes.

(E) Polarized HepG2-MDR1 cells were infected with HDAd-TFEB and then exposed to 200 μM $CuSO_4$ for 8 hr and loaded with CS3.

(F) 3D plots show the intensity of the CS3 signal in the corresponding canalicular areas (dash line in D).

(G) Levels of CS3 fluorescence within canalicular cysts of HepG2 cells (mean ± SD; n = 100 cysts) increased in cells overexpressing TFEB.

(H) Polarized HepG2-MDR1 cells were infected with HDAs-TFEB and treated with $CuSO_4$ as in (E). Afterward, canalicular cysts were opened with EDTA and their content was analyzed for Cu using ICP-MS. Normalized Cu concentration (mean ± SD; n = 3 experiments) increased in the biliary cysts of cells over-expressing TFEB.

The scale bars represent 7.5 μm (A) and 4 μm (D and E).

Activation of Lysosomal Exocytosis Accelerates Cell Surface Delivery of the Most Frequent Wilson-Disease-Causing ATP7B Mutant

Finally, we determined whether activation of lysosomal exocytosis could be utilized as a therapeutic strategy to contrast Wilson disease (WD) pathogenesis. The most frequent ATP7B mutant H1069Q (up to 50% in Caucasian population; Payne et al., 1998), exhibits residual catalytic activity (van den Berghe et al., 2009) but is retained within the endoplasmic reticulum (ER), where it undergoes degradation (Payne et al., 1998; van

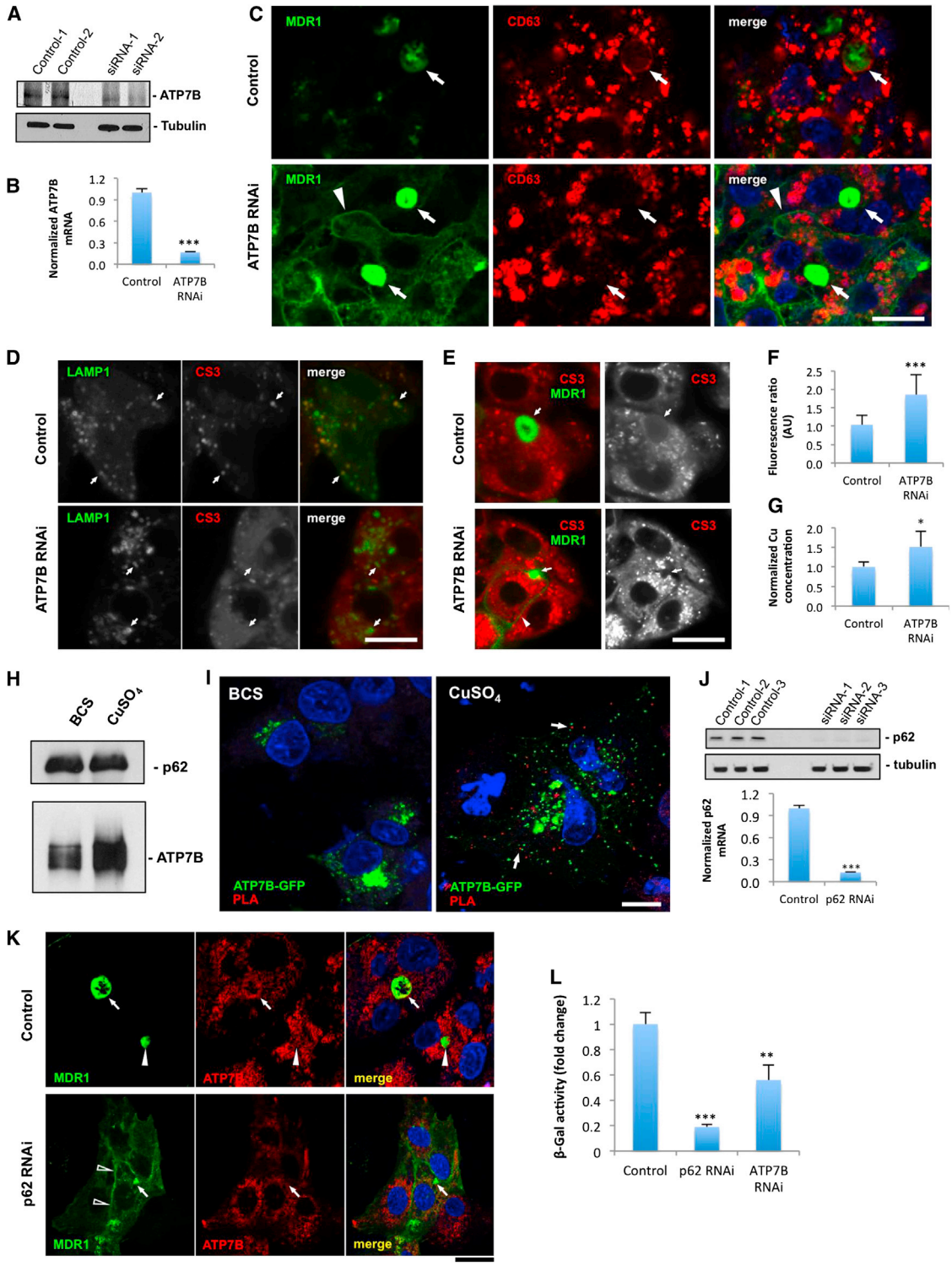

Figure 7. ATP7B Regulates Lysosomal Exocytosis and Cu Excretion through Interaction with p62

(A) Western blot reveals reduction in ATP7B expression in HepG2-MDR1 incubated with ATP7B-specific siRNAs.

(B) qRT-PCR indicates reduction of ATP7B mRNA levels (mean ± SD; n = 3 experiments) in ATP7B-silenced cells.

(C) Polarized control and ATP7B-silenced HepG2-MDR1 cells were exposed to 200 μM $CuSO_4$ for 8 hr, fixed, and stained for CD63. Arrows indicate apical cysts whereas arrowheads show MDR1 mistargeting from the canalicular area.

(D) Control and ATP7B-silenced HepG2 cells were transfected with LAMP1-GFP, exposed to $CuSO_4$, and loaded with CS3. Arrows indicate LAMP1-positive structures.

(legend continued on next page)

den Berghe et al., 2009). Thus, correction of this mutant to the regular functional compartment might be beneficial for the large cohort of the WD patients. Interestingly, despite extensive retention within the ER (Figures 8A and 8B, arrows), some ATP7B^{H1069Q} gets transported to the Golgi (empty arrows in Figures 8A and 8B) and further to LAMP1-positive structures (Figure 8A, solid arrows). Thus, we reasoned that acceleration of lysosomal exocytosis might allow a more-efficient supply of residual ATP7B^{H1069Q} to the cell surface, where it can transport Cu out of the cell. To test this, TFEB-overexpressing CF7 cells were infected with an adenovirus carrying ATP7B^{H1069Q} and exposed to $CuSO_4$. Arrows in Figure 8A show that exocytosis-prone lysosomes, which reside near the surface of CF7 cells (Medina et al., 2011), received ATP7B^{H1069Q}. This coincided with a stronger immunogold labeling of the mutant protein at the surface of CF7 cells compared to the parental HeLa line (Figures 8B, arrowheads, and 8C). Correspondingly, a biotinylation assay revealed a significant increase in the amount of ATP7B^{H1069Q} at the surface of CF7 cells (Figure 8D). Therefore, activation of lysosomal exocytosis allowed recovery of additional quantities of ATP7B^{H1069Q} at the cell surface.

To verify this conclusion in a liver-relevant system, polarized HepG2 cells expressing ATP7B^{H1069Q} were infected with HDAd-TFEB and exposed to $CuSO_4$ for 8 hr. Confocal microscopy revealed that, in control cells, ATP7B^{H1069Q} was hardly detectable within the MRP2-positive canalicular cysts, whereas overexpression of TFEB stimulated delivery of the mutant ATP7B toward the canalicular domain of hepatocytes (Figure 8E, arrows). Therefore, activation of lysosomal exocytosis allows recovery of additional amounts of ATP7B^{H1069Q} at the cell surface.

DISCUSSION

Our findings indicate that exposure of hepatocytes to increasing Cu concentrations induces ATP7B trafficking from the TGN to subset of lysosomes, where ATP7B imports Cu into the lysosomal lumen and where the metal can be transiently stored. Further Cu increase over a threshold value (approximately 20 μM) induces the exocytosis of lysosomes containing ATP7B with subsequent delivery of the Cu transporter to the apical surface of hepatocytes and the release of Cu into the biliary space. Importantly, ATP7B determines both the ability of the lysosome to undergo exocytosis and also the apical/canalicular direction of the exocytic process. Apparently, exocytosis is triggered by Cu-dependent interaction of ATP7B with p62 (DNCT4), which allows ATP7B to anchor lysosomes on microtubule highways directed toward the apical pole of hepatocytes. In our view, this sequence of events outlines the main mechanism, which is utilized by hepatocytes to remove excess Cu from liver and which is affected by ATP7B mutations in Wilson disease.

Some signs of this mechanism were uncovered more than 20 years ago when lysosomes were suggested to operate in Cu homeostasis (Gross et al., 1989). Later, ATP7B was even detected in late endosomes (Harada et al., 2000, 2005), and its involvement in the secretion of some lysosomal enzymes into bile was reported (Sugawara et al., 1995). Unfortunately, the conclusive experiments that would directly demonstrate a role of lysosomal exocytosis in ATP7B trafficking, molecular mechanisms behind this process, and its coordination with Cu excretion were not performed. Therefore, above findings remained mostly neglected over the last decade. This happened mainly because ATP7B trafficking and compartmentalization, which constitutes the centerpiece of Cu homeostasis in liver, remained poorly understood and highly controversial (La Fontaine and Mercer, 2007; Polishchuk and Lutsenko, 2013). The major mystery in the field was the nature of so-called "vesicles," where ATP7B resides in high-Cu conditions and how such vesicles operate in Cu excretion.

In this study, identification of the ATP7B transport itinerary allowed us to close these gaps and to complete the puzzle of the mechanism at the basis of Cu excretion in hepatocytes. Our initial finding revealed a subpopulation of lysosomes as the main intermediate in ATP7B trafficking. We demonstrated lysosomes to receive ATP7B directly from the TGN in response to increasing Cu and to actively use this pump for Cu import. This allowed us to assign the elusive "vesicular" ATP7B compartment with identity of the lysosomes.

The lysosomal localization of ATP7B in high Cu conditions raises several issues regarding the ATP7B-dependent mechanisms of Cu homeostasis. The first is whether Cu is required in the lysosome or it is merely sequestered there. Cu in lysosomes can be utilized as a cofactor by housekeeping enzymes (acid sphingomyelinase) (Qiu et al., 2003). Interestingly, another Cu pump, ATP7A, supplies the metal in a similar way to tyrosinase across the membrane of lysosome-related organelles melanosomes (Setty et al., 2008). ATP7A was also found to transport Cu into LAMP1/Rab7-positive phagosomes of macrophages, where the metal has been hypothesized to kill engulfed bacteria

(E) Control and ATP7B-silenced HepG2-MDR1 cells were treated with 200 μM $CuSO_4$ for 8 hr and loaded with CS3. Arrows show MDR1-positive canalicular vacuoles.
(F) Ratio between intracellular and canalicular CS3 fluorescence (mean ± SD; n = 100 cells) increased in ATP7B-deficient cells.
(G) Cells were treated like in (E) and prepared for ICP-MS, which revealed an increase in normalized Cu concentration (average ± SD; n = 4 experiments) upon ATP7B depletion.
(H) HepG2 cells were infected with adeno-ATP7B-GFP, exposed to BCS and or $CuSO_4$, lysed, and subjected to immunoprecipitation with anti-p62 antibody. Western blot reveals that similar amount of p62 pulls down higher amount of ATP7B in $CuSO_4$-treated cells.
(I) The cells were infected and treated like in (A) and processed for PLA analysis (see Experimental Procedures). PLA signal indicating close association of ATP7B and p62 was detectable as red spots (arrows) only in $CuSO_4$-treated cells.
(J) Western blot and qRT-PCR indicate reduction of p62 at both protein and mRNA levels in HepG2-MDR1 cells incubated with p62-specific siRNAs.
(K) Control and p62-silenced polarized HepG2-MDR1 cells were exposed to $CuSO_4$, fixed, and stained for endogenous ATP7B. Arrows indicate canalicular cysts. Empty arrowheads indicate MDR1 mistargeting from the canalicular area.
(L) Control, p62-silenced, or ATP7B-silenced HepG2 cells were exposed to CuSO4 for 8 hr. The chart shows decrease of normalized activity of β-Gal (mean ± SD; n = 3 experiments) in the canalicular cysts upon depletion of either p62 or ATP7B.
The scale bars represent 4 μm (C–E), 3 μm (I), and 5.2 μm (K).

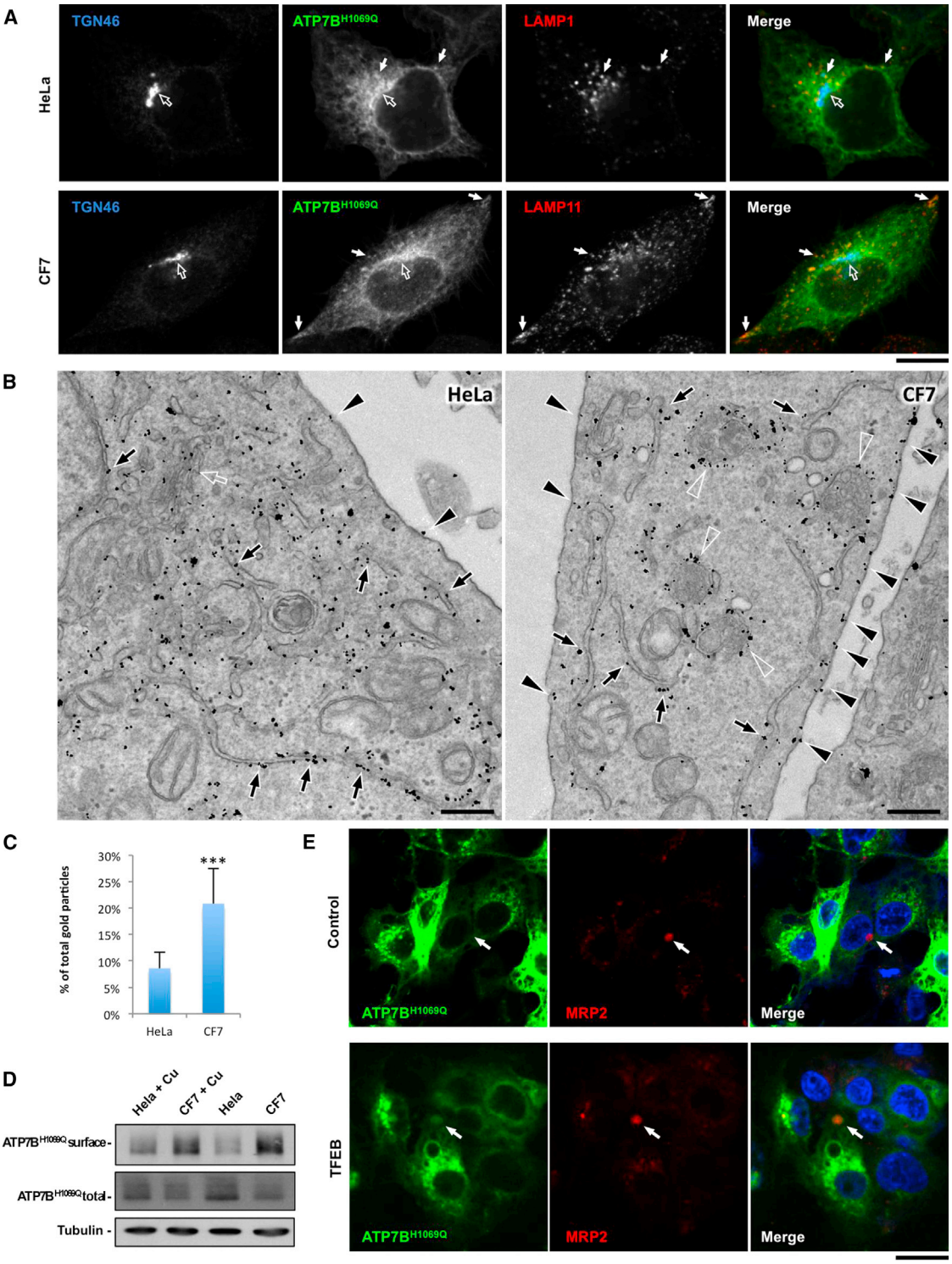

Figure 8. Activation of Lysosomal Exocytosis Improves Delivery of Most-Frequent WD-Causing ATP7B^{H1069Q} Mutant to the Cell Surface

(A) Control HeLa cells and CF7 cells were infected with adeno-ATP7B^{H1069Q}-GFP, incubated with 200 μM $CuSO_4$ for 2 hr, and stained for LAMP1 and TGN 46. Open and solid arrows show Golgi and lysosomes, respectively.

(B) Control HeLa and CF7 cells were treated as in (A), fixed, and processed for immunogold EM to reveal ATP7B^{H1069Q} distribution. Although ATP7B^{H1069Q} was mistargeted to the ER (arrows), it can be detected also in the Golgi (empty arrow) and lysosomes (empty arrowheads). Filled arrowheads indicate higher amount of ATP7B^{H1069Q} at the surface of CF7 cells.

(C) Quantification revealed increase in the percentage of ATP7B-associated gold particles (average ± SD; n = 30 cells) at the plasma membrane in CF7 cells.

(legend continued on next page)

(White et al., 2009). Thus, the ability to reach the lysosomal compartment and to function there could be a common feature of both Cu ATPases. Importantly, low pH in the lysosomes does not inhibit metal-transporting activity of ATP7B but favors it (Safaei et al., 2008).

The second issue is whether liver lysosomes may operate as Cu storage compartments. Our data suggest that lysosomes can uptake excess Cu from the cytosol through ATP7B (Figure 6), whereas the release of Cu in the opposite direction could occur through the lysosome-targeted Cu channel CTR2 (van den Berghe et al., 2007) when this metal is needed in the cytosol. We found that, at the Cu concentrations below 20 μM, ATP7B reaches the lysosomes from the TGN, but these lysosomes do not undergo exocytosis unless Cu levels increase further. This probably allows the ATP7B lysosomes to transiently store Cu, when its concentration does not yet threat cell homeostasis. Therefore, Cu fluxes to and from the lysosomes and, hence, Cu storage in these organelles should be tightly regulated. Indeed, yeast cells utilize vacuole (lysosome analog) for Cu storage (Nevitt et al., 2012), indicating that this function of lysosomes is conserved in evolution.

The third issue is whether an ATP7B-positive subset of lysosomes resembles lysosome-related organelles (LROs), which discharge their content in response to specific stimuli (Raposo et al., 2007). This property may be required for rapid release of Cu from the lysosome lumen into the bile in response to Cu overload. However, we found that neither Rab27A nor VAMP7 nor synaptotagmin7 depletion affected exocytosis of ATP7B-positive structures (Figure S5). Thus, in terms of exocytosis, ATP7B-positive lysosomes do not resemble LROs, which require Rab27A (Raposo et al., 2007). On the other hand, ATP7B-positive lysosomes share only some common elements of the exocytic molecular machinery (Ca^{2+} and MCOLN1) with common lysosomes, which need VAMP7 and synaptotagmin7 for exocytosis. In our view, the lysosomes may require a specific and unique asset of molecules for apical exocytosis in hepatocytes. ATP7B itself may be a part of such specific machinery, as it is expressed almost exclusively in hepatic cells (Lutsenko et al., 2007).

In this context, another significant finding of our study indicates lysosomal exocytosis to operate for both ATP7B and Cu delivery to the biliary surface of hepatocytes. Lysosomal exocytosis plays a major role in several physiological processes such as cellular immune response, bone resorption, and PM repair (Andrews, 2000). Our in vitro and in vivo data suggest that stimulation of lysosomal exocytosis increases both ATP7B and Cu in biliary cysts. Thus, it turns out that exocytosis of the lysosomes allows hepatocytes to expel sequestered Cu and to deliver ATP7B to canalicular surface, where it might pump Cu directly from the cytosol into the bile (Hubbard and Braiterman, 2008).

Our discovery of the ATP7B trafficking mechanism poses new questions. The first question addresses the way in which Cu triggers exocytosis of the lysosomes that receive ATP7B. We found that ATP7B ablation inhibits lysosome clustering and the release of lysosomal content at the biliary surface (Figures 7C and 7L). In line with these observations, ATP7B-deficient rats exhibit significant decrease of lysosome enzyme activity in the bile (Sugawara et al., 1995), presumably due to suppression of lysosomal exocytosis in the absence of functional ATP7B. Thus, the presence of ATP7B probably defines whether a given lysosome has to undergo exocytosis in hepatocytes when Cu increases. Moreover, ATP7B also determines the apical/canalicular direction of such exocytosis. We found that the ability of ATP7B to drive exocytic processes in response to Cu is likely governed by ATP7B's interaction with the p62. p62 interacts with ATP7B in the presence of high Cu (Lim et al., 2006; see also Figures 7H and 7I) and therefore, being in complex with dynactin and dynein motor, can probably pull ATP7B-enriched lysosomes to the microtubule minus ends, which are oriented toward the canalicular domain of hepatocytes (Cohen et al., 2004). Indeed, we observed that depletion of p62 does not allow ATP7B-containing lysosomes to move toward the apical pole of HepG2 cells and to deliver ATP7B to the canalicular surface, even in the presence of excess Cu (see Figure 7). These findings are in line with previous studies showing microtubule disruption to impair delivery of ATP7B to the canalicular surface of HepG2 cells (Roelofsen et al., 2000). Our observations also indicate that ATP7B-mediated lysosomal exocytosis may contribute to polarization of hepatic cells (Figure S4), likely facilitating the delivery of specific proteins and lipids to the apical membrane domain. Partial disorganization of liver architecture and hepatic tumor development in ATP7B-deficient mice (Huster et al., 2006) argues in favor of this hypothesis.

The second question is whether and how the lysosome exocytosis pathway may be utilized for therapeutic purposes. Stimulation of lysosomal exocytosis via TFEB overexpression has already been shown to promote cellular clearance in lysosomal storage diseases (Medina et al., 2011). Here, we found that transcriptional activation of lysosomal exocytosis allows partial recovery of the proper subcellular localization of the most frequent WD-causing mutant to the regular ATP7B functional site. Given that this mutant possesses significant residual Cu-transporting activity (van den Berghe et al., 2009), its rescue to the correct location on the biliary surface of hepatocytes could be beneficial for a large cohort of WD patients. On the other hand, toxic Cu accumulation in lysosomes has been reported during pathogenesis of choleostatic disorders (Gross et al., 1989) and could be probably circumvented (contrasted) through activation of the lysosome fusion with the cell membrane. In addition, the well-known role of ATP7B in Wilson disease has been recently expanded to its involvement in other pathologies such as modulation of the Alzheimer's disease phenotype and anticancer drug resistance (Gupta and Lutsenko, 2009). Thus, the ATP7B-dependent lysosomal exocytosis emerges as a promising therapeutic target to combat WD and a number of other disorders.

(D) HeLa and CF7 cells were infected with adeno-ATP7B^{H1069Q}-GFP and then prepared for surface biotinylation directly or 2 hr after stimulation with 200 μM $CuSO_4$. Western blot revealed higher amount of ATP7B at the surface of CF7 cells.
(E) Polarized HepG2 cells expressing ATP7B^{H1069Q}-GFP were infected with HDAd-TFEB, incubated with 200 μM $CuSO_4$ for 8 hr, and stained with canalicular marker MRP2. Arrows indicate canalicular cyst.
The scale bars represent 3.8 μm (A), 240 nm (B), and 6.5 μm (E).

EXPERIMENTAL PROCEDURES

Cell Culture and Transfection and Construction of Recombinant Adenoviruses

HepG2, HepG2-MDR1, HeLa, and HeLa CF7 cells were grown in Dulbecco's modified Eagle's medium supplemented with 10% fetal calf serum (decomplemented for HepG2), 2 mM L-glutamine, penicillin, and streptomycin. For transfection of plasmids, jetPEI TM-Hepatocyte (Polyplus transfection) and Trans IT LT1 (Tema Ricerca SRL) transfection reagents were used for HepG2 and HeLa, respectively.

Trafficking Assay and Cu Treatment

To investigate localization of ATP7B at the different Cu load, cells were treated with 200 μM Cu-chelating agent BCS and with different concentrations of $CuSO_4$. To compare trafficking of ATP7B with VSVG, cells were incubated with BCS (overnight), then infected with VSV (Polishchuk et al., 2003), incubated at 20°C in the presence of BCS (to accumulate both proteins in the Golgi), and finally warmed to 32°C and treated with $CuSO_4$ (to activate post-Golgi transport of both proteins). Tannic acid (0.5%) was added in some experiments during release of 20°C block to inhibit fusion of post-Golgi transport carriers with the PM (Polishchuk et al., 2004).

Mice and Treatment

Two-month-old males of *Tcfeb*-flox mouse (Settembre et al., 2013) were used. TcFEB loxP/loxP mice that did not carry the albumin Cre were utilized as a control. To express ATP7B-GFP, mice were subjected to retro-orbital injection with adeno-ATP7B-GFP 3 days before the experiment. To stimulate Cu excretion from liver, both control and *Tcfeb*-flox mice received 0.125% $CuSO_4$ in water 4 hr before the animals were sacrificed (Gross et al., 1989). Liver tissue was rapidly dissected from the mice, fixed, and processed for electron microscopy, whereas bile was collected from gall bladder for β-Gal and β-Hex assays. All experiments were approved by the Committee on Animal Care at Baylor College of Medicine and conform to the legal mandates and federal guidelines for the care and maintenance of laboratory animals.

Immunofluorescence and CS3 Labeling

Cells were fixed for 10 min with 4% paraformaldehyde in 0.2 M HEPES, permeabilized, labeled with primary and secondary antibodies, and examined with a ZEISS LSM 700 or LSM 710 confocal microscope equipped with a 63× 1.4 numerical aperture oil objective. For fluorescent Cu detection, cells were incubated with 5 μM CS3 solution for 15 min at 37°C. CS3 was excited with 561 nm laser of LSM710, and its emission was collected from 565 to 650 nm. Colocalization module of ZEISS ZEN 2008 software was used to measure colocalization of ATP7B with different intracellular markers. ATP7B fluorescent signal inside canalicular domains and CS3 cytosolic and canalicular surface signals were measured using ZEISS ZEN 2008 software and reported in arbitrary units.

Immunoelectron Microscopy

For pre-embedding immunoelectron microscopy, cells were fixed, permeabilized, and labeled as described previously (Polishchuk et al., 2003). For cryo-immunoelectron microscopy, specimens were fixed, frozen, and cut using Leica EM FC7 ultramicrotome. Cryo sections were double labeled for LAMP1 and GFP. EM images were acquired using a FEI Tecnai-12 electron microscope. Morphometric analyses were performed using iTEM software (Olympus SIS).

Statistical Analyses

Data are expressed as mean values ± SD. Statistical significance was computed using the Student's two-tail t test. A p value < 0.05 was considered statistically significant. In all figures, *$p < 0.05$, **$p < 0.01$, and ***$p < 0.001$.

Additional Methods

Additional information on DNA constructs, adenoviruses, antibodies, immunoprecipitation, surface biotinylation, PLA, quantitative RT-PCR (qRT-PCR), RNAi, determination of β-Gal and β-Hex activities, atomic adsorption spectroscopy (AAS), and ICP-MS is provided in the Supplemental Experimental Procedures.

SUPPLEMENTAL INFORMATION

Supplemental Information includes Supplemental Experimental Procedures and five figures and can be found with this article online at http://dx.doi.org/10.1016/j.devcel.2014.04.033.

ACKNOWLEDGMENTS

This work was supported by grants from Italian Telethon Foundation (TGM11CB4 to R.S.P., TGM11SB1 to A.B., P37TELC to N.B.-P., and TCP12008 to C.S.), AIRC (IG 10233 to R.S.P.), ERC (250154 to A.B. and IEMTx to N.B.-P.), March of Dimes (no. 6-FY11-306 to A.B.), and NIH (R01-NS078072 to A.B.). C.J.C. is an Investigator with the Howard Hughes Medical Institute and thanks support from the NIH (GM 79465). G.C. and J.C. were supported by a fellowship from POR Campania and HFSP, respectively. We would like to acknowledge support from Associazione Nazionale Malattia di Wilson and everybody who provided us with antibodies, reagents, and cells. We would like to thank Svetlana Lutsenko, Graciana Diez-Roux, and Antonella De Matteis for critical reading of the manuscript, TIGEM Advanced Microscopy and Imaging Core for microscopy support, and TIGEM Vector Core for production of adenoviruses.

Received: October 1, 2013
Revised: March 15, 2014
Accepted: April 29, 2014
Published: June 5, 2014

REFERENCES

Andrews, N.W. (2000). Regulated secretion of conventional lysosomes. Trends Cell Biol. *10*, 316–321.

Cater, M.A., La Fontaine, S., Shield, K., Deal, Y., and Mercer, J.F. (2006). ATP7B mediates vesicular sequestration of copper: insight into biliary copper excretion. Gastroenterology *130*, 493–506.

Cohen, D., Brennwald, P.J., Rodriguez-Boulan, E., and Müsch, A. (2004). Mammalian PAR-1 determines epithelial lumen polarity by organizing the microtubule cytoskeleton. J. Cell Biol. *164*, 717–727.

D'Agostino, M., Lemma, V., Chesi, G., Stornaiuolo, M., Cannata Serio, M., D'Ambrosio, C., Scaloni, A., Polishchuk, R., and Bonatti, S. (2013). The cytosolic chaperone α-crystallin B rescues folding and compartmentalization of misfolded multispan transmembrane proteins. J. Cell Sci. *126*, 4160–4172.

Dodani, S.C., Domaille, D.W., Nam, C.I., Miller, E.W., Finney, L.A., Vogt, S., and Chang, C.J. (2011). Calcium-dependent copper redistributions in neuronal cells revealed by a fluorescent copper sensor and X-ray fluorescence microscopy. Proc. Natl. Acad. Sci. USA *108*, 5980–5985.

Gross, J.B., Jr., Myers, B.M., Kost, L.J., Kuntz, S.M., and LaRusso, N.F. (1989). Biliary copper excretion by hepatocyte lysosomes in the rat. Major excretory pathway in experimental copper overload. J. Clin. Invest. *83*, 30–39.

Guo, Y., Nyasae, L., Braiterman, L.T., and Hubbard, A.L. (2005). NH2-terminal signals in ATP7B Cu-ATPase mediate its Cu-dependent anterograde traffic in polarized hepatic cells. Am. J. Physiol. Gastrointest. Liver Physiol. *289*, G904–G916.

Gupta, A., and Lutsenko, S. (2009). Human copper transporters: mechanism, role in human diseases and therapeutic potential. Future Med. Chem. *1*, 1125–1142.

Harada, M., Sakisaka, S., Kawaguchi, T., Kimura, R., Taniguchi, E., Koga, H., Hanada, S., Baba, S., Furuta, K., Kumashiro, R., et al. (2000). Copper does not alter the intracellular distribution of ATP7B, a copper-transporting ATPase. Biochem. Biophys. Res. Commun. *275*, 871–876.

Harada, M., Kawaguchi, T., Kumemura, H., Terada, K., Ninomiya, H., Taniguchi, E., Hanada, S., Baba, S., Maeyama, M., Koga, H., et al. (2005). The Wilson disease protein ATP7B resides in the late endosomes with Rab7 and the Niemann-Pick C1 protein. Am. J. Pathol. *166*, 499–510.

Hasan, N.M., Gupta, A., Polishchuk, E., Yu, C.H., Polishchuk, R., Dmitriev, O.Y., and Lutsenko, S. (2012). Molecular events initiating exit of a

copper-transporting ATPase ATP7B from the trans-Golgi network. J. Biol. Chem. *287*, 36041–36050.

Hirst, J., Borner, G.H., Antrobus, R., Peden, A.A., Hodson, N.A., Sahlender, D.A., and Robinson, M.S. (2012). Distinct and overlapping roles for AP-1 and GGAs revealed by the "knocksideways" system. Curr. Biol. *22*, 1711–1716.

Hubbard, A.L., and Braiterman, L.T. (2008). Could ATP7B export Cu(I) at the tight junctions and the apical membrane? Gastroenterology *134*, 1255–1257.

Huster, D., Finegold, M.J., Morgan, C.T., Burkhead, J.L., Nixon, R., Vanderwerf, S.M., Gilliam, C.T., and Lutsenko, S. (2006). Consequences of copper accumulation in the livers of the Atp7b-/- (Wilson disease gene) knockout mice. Am. J. Pathol. *168*, 423–434.

La Fontaine, S., and Mercer, J.F. (2007). Trafficking of the copper-ATPases, ATP7A and ATP7B: role in copper homeostasis. Arch. Biochem. Biophys. *463*, 149–167.

La Fontaine, S., Theophilos, M.B., Firth, S.D., Gould, R., Parton, R.G., and Mercer, J.F. (2001). Effect of the toxic milk mutation (tx) on the function and intracellular localization of Wnd, the murine homologue of the Wilson copper ATPase. Hum. Mol. Genet. *10*, 361–370.

Lim, C.M., Cater, M.A., Mercer, J.F., and La Fontaine, S. (2006). Copper-dependent interaction of dynactin subunit p62 with the N terminus of ATP7B but not ATP7A. J. Biol. Chem. *281*, 14006–14014.

Lutsenko, S. (2010). Human copper homeostasis: a network of interconnected pathways. Curr. Opin. Chem. Biol. *14*, 211–217.

Lutsenko, S., Barnes, N.L., Bartee, M.Y., and Dmitriev, O.Y. (2007). Function and regulation of human copper-transporting ATPases. Physiol. Rev. *87*, 1011–1046.

Medina, D.L., Fraldi, A., Bouche, V., Annunziata, F., Mansueto, G., Spampanato, C., Puri, C., Pignata, A., Martina, J.A., Sardiello, M., et al. (2011). Transcriptional activation of lysosomal exocytosis promotes cellular clearance. Dev. Cell *21*, 421–430.

Nevitt, T., Ohrvik, H., and Thiele, D.J. (2012). Charting the travels of copper in eukaryotes from yeast to mammals. Biochim. Biophys. Acta *1823*, 1580–1593.

Payne, A.S., Kelly, E.J., and Gitlin, J.D. (1998). Functional expression of the Wilson disease protein reveals mislocalization and impaired copper-dependent trafficking of the common H1069Q mutation. Proc. Natl. Acad. Sci. USA *95*, 10854–10859.

Polishchuk, R., and Lutsenko, S. (2013). Golgi in copper homeostasis: a view from the membrane trafficking field. Histochem. Cell Biol. *140*, 285–295.

Polishchuk, E.V., Di Pentima, A., Luini, A., and Polishchuk, R.S. (2003). Mechanism of constitutive export from the golgi: bulk flow via the formation, protrusion, and en bloc cleavage of large trans-golgi network tubular domains. Mol. Biol. Cell *14*, 4470–4485.

Polishchuk, R., Di Pentima, A., and Lippincott-Schwartz, J. (2004). Delivery of raft-associated, GPI-anchored proteins to the apical surface of polarized MDCK cells by a transcytotic pathway. Nat. Cell Biol. *6*, 297–307.

Pols, M.S., van Meel, E., Oorschot, V., ten Brink, C., Fukuda, M., Swetha, M.G., Mayor, S., and Klumperman, J. (2013). hVps41 and VAMP7 function in direct TGN to late endosome transport of lysosomal membrane proteins. Nat. Commun. *4*, 1361.

Qiu, H., Edmunds, T., Baker-Malcolm, J., Karey, K.P., Estes, S., Schwarz, C., Hughes, H., and Van Patten, S.M. (2003). Activation of human acid sphingomyelinase through modification or deletion of C-terminal cysteine. J. Biol. Chem. *278*, 32744–32752.

Raposo, G., Marks, M.S., and Cutler, D.F. (2007). Lysosome-related organelles: driving post-Golgi compartments into specialisation. Curr. Opin. Cell Biol. *19*, 394–401.

Roelofsen, H., Wolters, H., Van Luyn, M.J., Miura, N., Kuipers, F., and Vonk, R.J. (2000). Copper-induced apical trafficking of ATP7B in polarized hepatoma cells provides a mechanism for biliary copper excretion. Gastroenterology *119*, 782–793.

Safaei, R., Otani, S., Larson, B.J., Rasmussen, M.L., and Howell, S.B. (2008). Transport of cisplatin by the copper efflux transporter ATP7B. Mol. Pharmacol. *73*, 461–468.

Saftig, P., and Klumperman, J. (2009). Lysosome biogenesis and lysosomal membrane proteins: trafficking meets function. Nat. Rev. Mol. Cell Biol. *10*, 623–635.

Settembre, C., De Cegli, R., Mansueto, G., Saha, P.K., Vetrini, F., Visvikis, O., Huynh, T., Carissimo, A., Palmer, D., Klisch, T.J., et al. (2013). TFEB controls cellular lipid metabolism through a starvation-induced autoregulatory loop. Nat. Cell Biol. *15*, 647–658.

Setty, S.R., Tenza, D., Sviderskaya, E.V., Bennett, D.C., Raposo, G., and Marks, M.S. (2008). Cell-specific ATP7A transport sustains copper-dependent tyrosinase activity in melanosomes. Nature *454*, 1142–1146.

Slimane, T.A., Trugnan, G., Van IJzendoorn, S.C., and Hoekstra, D. (2003). Raft-mediated trafficking of apical resident proteins occurs in both direct and transcytotic pathways in polarized hepatic cells: role of distinct lipid microdomains. Mol. Biol. Cell *14*, 611–624.

Sugawara, N., Sato, M., Yuasa, M., and Sugawara, C. (1995). Biliary excretion of copper, metallothionein, and glutathione into Long-Evans Cinnamon rats: a convincing animal model for Wilson disease. Biochem. Mol. Med. *55*, 38–42.

van den Berghe, P.V., Folmer, D.E., Malingré, H.E., van Beurden, E., Klomp, A.E., van de Sluis, B., Merkx, M., Berger, R., and Klomp, L.W. (2007). Human copper transporter 2 is localized in late endosomes and lysosomes and facilitates cellular copper uptake. Biochem. J. *407*, 49–59.

van den Berghe, P.V., Stapelbroek, J.M., Krieger, E., de Bie, P., van de Graaf, S.F., de Groot, R.E., van Beurden, E., Spijker, E., Houwen, R.H., Berger, R., and Klomp, L.W. (2009). Reduced expression of ATP7B affected by Wilson disease-causing mutations is rescued by pharmacological folding chaperones 4-phenylbutyrate and curcumin. Hepatology *50*, 1783–1795.

White, C., Lee, J., Kambe, T., Fritsche, K., and Petris, M.J. (2009). A role for the ATP7A copper-transporting ATPase in macrophage bactericidal activity. J. Biol. Chem. *284*, 33949–33956.

Bibliography

Alexander MS, Casar JC, Motohashi N, Myers JA, Eisenberg I, Gonzalez RT, Estrella EA, Kang PB, Kawahara G, Kunkel LM: Regulation of DMD pathology by an ankyrin-encoded miRNA. Skelet Muscle. 2011 Aug 8;1:27. doi: 10.1186/2044-5040-1-27.

Allegra A, Alonci A, Campo S, Penna G, Petrungaro A, Gerace D, Musolino C: Circulating microRNAs: new biomarkers in diagnosis, prognosis and treatment of cancer (review). International journal of oncology 2012, 41(6):1897-1912.

Amalfitano A, Bengur AR, Morse RP, Majure JM, Case LE, Veerling DL, Mackey J, Kishnani P, Smith W, McVie-Wylie A, Sullivan JA, Hoganson GE, Phillips JA 3rd, Schaefer GB, Charrow J, Ware RE, Bossen EH, Chen YT: Recombinant human acid alpha-glucosidase enzyme therapy for infantile glycogen storage disease type II: results of a phase I/II clinical trial. *Genet Med* 2001, 3:132-138.

Ana C. Liberman, Jimena Druker, Marcelo J. Perone, Eduardo Arzt. Glucocorticoids in the regulation of trascription factors that control cytokyne synthesis. Cytokine and Growth Factor Rewiews 18 (2007) 45-56.

Angelini C, Semplicini C, Ravaglia S, Moggio M, Comi GP, Musumeci O, Pegoraro E, Tonin P, Filosto M, Servidei S, Morandi L, Crescimanno G, Marrosu G, Siciliano G, Mongini T, Toscano A; Italian Group on GSDII. New motor outcome function measures in evaluation of late-onset Pompe disease before and after enzyme replacement therapy. Muscle Nerve. 2012 Jun;45(6):831-4 Bartel DP: MicroRNAs: genomics, biogenesis, mechanism, and function. Cell 2004, 116(2):281-297

Bach JR, Martinez D, Saulat B: Duchenne muscular dystrophy: the effect of glucocorticoids on ventilator use and ambulation. *Am J Phys Med Rehabil* 89: 620-624, 2010.

Bartel DP: MicroRNAs: target recognition and regulatory functions. Cell 2009, 136(2):215-233.

Biggar WD, Harris VA, Eliasoph L, Alman B. Long-term benefits of deflazacort 16. treatment for boys with Duchenne muscular dystrophy in their second decade. Neuromuscul Disord 2006;16:249-255.

Bosca´, L., M. Zeini, P. G. Trave´s, and S. Hortelano. 2005. Nitric oxide and cell viability in inflammatory cells: a role for NO in macrophage function and fate. *Toxicology* 208: 249–258.

Brady RO (2006) Enzyme replacement for lysosomal diseases. Annu Rev Med 57:283-296

Bushati N, Cohen SM: microRNA functions. Annual review of cell and developmental biology 2007, 23:175-205.

Butters TD, Dwek RA, Platt FM (2005) Imino sugar inhibitors for treating the lysosomal glycosphingolipidoses. Glycobiology 15:43R-52R

Cacchiarelli D, Legnini I, Martone J, Cazzella V, D'Amico A, Bertini E, Bozzoni I: miRNAs as serum biomarkers for Duchenne muscular dystrophy. EMBO molecular medicine 2011, 3(5):258-265.

Chargè SB, Rudnicki MA: Cellular and molecular regulation of muscle regeneration. *Physiol Rev* 84: 209-238, 2004.

Cheng Y, Tan N, Yang J, Liu X, Cao X, He P, Dong X, Qin S, Zhang C: A translational study of circulating cell-free microRNA-1 in acute myocardial infarction. Clinical science 2010, 119(2):87-95.

Ciciliot S, Schiaffino S: Regeneration of mammalian skeletal muscle. Basic mechanisms and clinical implications. *Curr Pharm Des* 16: 906-914, 2010.

Croce CM: Causes and consequences of microRNA dysregulation in cancer. Nature reviews Genetics 2009, 10(10):704-714.

D'Alessandra Y, Devanna P, Limana F, Straino S, Di Carlo A, Brambilla PG, Rubino M, Carena MC, Spazzafumo L, De Simone M et al: Circulating microRNAs are new and sensitive biomarkers of myocardial infarction. European heart journal 2010, 31(22):2765-2773.

de Pontual L, Yao E, Callier P, Faivre L, Drouin V, Cariou S, Van Haeringen A, Genevieve D, Goldenberg A, Oufadem M et al: Germline deletion of the miR-17 approximately 92 cluster causes skeletal and growth defects in humans. Nature genetics 2011, 43(10):1026-1030.

Devaux Y, Vausort M, Goretti E, Nazarov PV, Azuaje F, Gilson G, Corsten MF, Schroen B, Lair ML, Heymans S et al: Use of circulating microRNAs to diagnose acute myocardial infarction. Clinical chemistry 2012, 58(3):559-567.

Djuranovic S, Nahvi A, Green R: miRNA-mediated gene silencing by translational repression followed by mRNA deadenylation and decay. Science 2012, 336(6078):237-240.

Dupont FO, Gagnon R, Boutin M, Auray-Blais C. A metabolomic study reveals novel plasma lyso-Gb3 analogs as Fabry disease biomarkers. Curr Med Chem. 2013;2

Einat B. Vitner‡, Frances M. Platt§, and Anthony H. Futerman Common and Uncommon Pathogenic Cascades in Lysosomal Storage Diseases. *The journal of biological chemistry*. July 2, 2010 vol 285, no. 27, pp 20423–20427.

Eng CM, Guffon N, Wilcox WR, Germain DP, Lee P, Waldek S, Caplan L, Linthorst GE, Desnick RJ; International Collaborative Fabry Disease Study Group. Safety and efficacy of recombinant human alpha-galactosidase A--replacement therapy in Fabry's disease. N Engl J Med. 2001 Jul 5;345(1):9-16

Eulalio A, Huntzinger E, Izaurralde E: Getting to the root of miRNA-mediated gene silencing. Cell 2008, 132(1):9-14.

Fabian MR, Sonenberg N: The mechanics of miRNA-mediated gene silencing: a look under the hood of miRISC. Nature structural & molecular biology 2012, 19(6):586-593.

Fan JQ, Ishii S, Asano N, Suzuki Y. Accelerated transport and maturation of lysosomal alpha-galactosidase A in Fabry lymphoblasts by an enzyme inhibitor. Nat Med. 1999 Jan;5(1):112-5

Fan JQ (2008) A counterintuitive approach to treat enzyme deficiencies: use of enzyme inhibitors for restoring mutant enzyme activity. Biol Chem 389(1):1-11

Fuller M, Meikle PJ, Hopwood JJ. Epidemiology of lysosomal storage diseases: an overview. In: Mehta A, Beck M, Sunder-Plassmann G, editors. Fabry Disease: Perspectives from 5 Years of FOS. Oxford: Oxford PharmaGenesis; 2006. Chapter 2

Gallagher PG, Forget BG: An alternate promoter directs expression of a truncated, muscle-specific isoform of the human ankyrin 1 gene. J Biol Chem 1998, 273:1339-1348.

Gilad S, Meiri E, Yogev Y, Benjamin S, Lebanony D, Yerushalmi N, Benjamin H, Kushnir M, Cholakh H, Melamed N et al: Serum microRNAs are promising novel biomarkers. PloS one 2008, 3(9):e3148.

Germain DP. Fabry disease. Orphanet J Rare Dis. 2010 Nov 22;5:30

Glass DJ: Signaling pathways perturbing muscle mass. *Curr Opin Clin Nutr Metab Care* 13: 225-229, 2010.

Gordon, S., and P. R. Taylor. 2005. Monocyte and macrophage heterogeneity. *Nat. Rev. Immunol*. 5: 953–964.
Hoefsloot LH, Hoogeveen-Westerveld M, Reuser AJ, Oostra BA. Characterization of the humanlysosomal alpha-glucosidase gene. Biochem J. 1990 Dec 1;272(2):493-7.

Hirschhorn R, Reuser AJJ: Glycogen storage disease type II: acid a-glucosidase (acid maltase) deficiency. In *The Metabolic and Molecular Bases of Inherited Disease* 8th edition. Edited by: Scriver CR, Beaudet AL, Valle D, Sly WS. New York: McGraw-Hill, Inc; 2001:3389-3420.

Hughes AE, Bradley DT, Campbell M, Lechner J, Dash DP, Simpson DA, Willoughby CE: Mutation altering the miR-184 seed region causes familial keratoconus with cataract. American journal of human genetics 2011, 89(5):628-633.

James G. Tidball: Inflammatory processes in muscle injury and repair. Am *J Physiol Regul Integr Comp Physiol.* 288:R345-R353, 2005.

Kaliman P, Canicio J, Testar X, Palacin M. Zorzno A: Insulin-like growth factor-II, phosphatidylinositol 3-kinase, nuclear factor-kappaB and inducibile nitric-oxide synthase define a common myogenic signaling pathway. J Biol Chem 1999, 274:17437-17444.

Karin M. The beginning of the end: IKappaB (IKK) and NF-kappaB activation. J Biol chem. 1999; 274:27339-42.

Kinet V, Halkein J, Dirkx E, Windt LJ: Cardiovascular extracellular microRNAs: emerging diagnostic markers and mechanisms of cell-to-cell RNA communication. Frontiers in genetics 2013, 4:214.

Kishnani PS, Howell RR: Pompe disease in infants and children.*J Pediatr* 2004, 144:S35-43.

Kishnani PS, Nicolino M, Voit T, Rogers RC, Tsai AC, Waterson J, Herman GE, Amalfitano A, Thurberg BL, Richards S, Davison M, Corzo D, Chen YT: Chinese hamster ovary cell-derived recombinant human acid alpha-glucosidase in infantile-onset Pompe disease. *J Pediatr* 2006, 149:89-97.

Kuwabara Y, Ono K, Horie T, Nishi H, Nagao K, Kinoshita M, Watanabe S, Baba O, Kojima Y, Shizuta S et al: Increased microRNA-1 and microRNA-133a levels in serum of patients with cardiovascular disease indicate myocardial damage. Circulation Cardiovascular genetics 2011, 4(4):446-454.

Lavoie P, Boutin M, Auray-Blais C. Multiplex analysis of novel urinary lyso-Gb3-related biomarkers for Fabry disease by tandem mass spectrometry. Anal Chem. 2013 Feb 5;85(3):1743-52

Lidove O, Bekri S, Goizet C, Khau Van Kien A, Aractingi S, Knebelmann B, Choukroun G, Tsimaratos M, Redonnet-Vernhet I, Lacombe D, Jaussaud R. [Fabry disease: proposed guidelines from a French expert group for its diagnosis, treatment and follow-up]. Presse Med. 2007 Jul-Aug;36(7-8):1084-97

Lidove O, West ML, Pintos-Morell G, Reisin R, Nicholls K, Figuera LE, Parini R, Carvalho LR, Kampmann C, Pastores GM, Mehta A. Effects of enzyme replacement therapy in Fabry disease--a comprehensive review of the medical literature. Genet Med. 2010 Nov;12(11):668-79

Ling H, Fabbri M, Calin GA: MicroRNAs and other non-coding RNAs as targets for anticancer drug development. Nature reviews Drug discovery 2013, 12(11):847-865.

Lombardo, E., A. Alvarez-Barrientos, B. Maroto, L. Bosca´, and U. G. Knaus. 2007. TLR4-mediated survival of macrophages is MyD88 dependent and requires TNF-a autocrine signalling. *J. Immunol.* 178: 3731–3739.

Ma Y, Zhang P, Wang F, Zhang H, Yang J, Peng J, Liu W, Qin H: miR-150 as a potential biomarker associated with prognosis and therapeutic outcome in colorectal cancer. Gut 2012, 61(10):1447-1453.

Mehta A, Beck M, Elliott P, Giugliani R, Linhart A, Sunder-Plassmann G, Schiffmann R, Barbey F, Ries M, Clarke JT; Fabry Outcome Survey investigators. Enzyme replacement therapy with agalsidase alfa in patients with Fabry's disease: an analysis of registry data. Lancet. 2009 Dec 12;374(9706):1986-96.

Mantovani, A., A. Sica, and M. Locati. 2005. Macrophage polarization comes of age. *Immunity* 23: 344–346.

Manwaring V, Boutin M, Auray-Blais C. A metabolomic study to identify new globotriaosylceramide-related biomarkers in the plasma of Fabry disease patients. Anal Chem. 2013 Oct 1;85(19):9039-48

Mahmoud Rezk A Hussein,1 Eman E Abu-Dief,2 Nageh Fouly Kamel,3 Mohammed G Mostafa. Steroid therapy is associated with decreased numbers of dendritic cells and fibroblasts, and increased numbers of satellite cells, in the dystrophic skeletal muscle. J Clin Pathol 2010;63:805e813.

Matthews DJ, James KA, Miller LA, Pandya S, Campbell KA, Ciafaloni E, Mathews KD, Miller TM, Cunniff C, Meaney FJ, Drushel CM, Romitti PA, Fox DJ; MD

STARNET: Use of corticosteroids in a population-based cohort of boys with duchenne and becker muscular dystrophy. *J Child Neurol* 25: 1319-1324, 2010.

Mencia A, Modamio-Hoybjor S, Redshaw N, Morin M, Mayo-Merino F, Olavarrieta L, Aguirre LA, del Castillo I, Steel KP, Dalmay T et al: Mutations in the seed region of human miR-96 are responsible for nonsyndromic progressive hearing loss. Nature genetics 2009, 41(5):609-613

Menconi M, Fareed M, O'neal P, Poylin V, Wei W, Hasselgren PO: Role of glucocorticoids in the molecular regulation of muscle wasting. *Crit Care Med* 35: S602-S608, 2007.

Mendell JR, Moxley RT, Griggs RC. Randomized double-blind six month trial of 13. prednisone in Duchenne muscular dystrophy. N Engl J Med 1989;320:1592-1597.

Mendell JT, Olson EN: MicroRNAs in stress signaling and human disease. Cell 2012, 148(6):1172-1187.

Mercuri, E, Pichiecchio, A, Counsell, S, Allsop, J, Cini, C, Jungbluth, H *et al*. (2002). A short protocol for muscle MRI in children with muscular dystrophies. *Eur J Paediat Neurol* **6**: 305-307.

Messina S, Vita GL, Aguennouz M, Sframeli M, Romeo S, Rodolico C, Vita G. Activation of NF-kB pathway in Duchenne muscular dystrophy: relation to age. Acta Myologica. 2011; xxx: p. 16-23.

Messina S, Altavilla M, Aguennouz M, Seminara P, Minutoli L, Monici MC, Bitto A, Mazzeo A, Marini H, Squadrito F, and Vita G: Lipid Peroxidation Inhibition Blunts Nuclear Factor-kB Activation, Reduces Skeletal Muscle Degeneration, and Enhances Muscle Function in mdx Mice. American Journal of pathology, Vol. 168, No. 3, March 2006.

Mitchell PS, Parkin RK, Kroh EM, Fritz BR, Wyman SK, Pogosova-Agadjanyan EL, Peterson A, Noteboom J, O'Briant KC, Allen A et al: Circulating microRNAs as stable blood-based markers for cancer detection. Proceedings of the National Academy of Sciences of the United States of America 2008, 105(30):10513-10518.

Nakao S, Kodama C, Takenaka T, Tanaka A, Yasumoto Y, Yoshida A, Kanzaki T, Enriquez AL, Eng CM, Tanaka H, Tei C, Desnick RJ. Fabry disease: detection of undiagnosed hemodialysis patients and identification of a "renal variant" phenotype. Kidney Int. 2003 Sep;64(3):801-7

Orchard PJ et al. (2007) Hematopoietic cell therapy for metabolic disease. J Pediatr 151:340-346

Parenti G, Andria G, Ballabio A: Lysosomal storage diseases: from pathophysiology to therapy. Annu Rev Med. 2015;66:471-86. doi: 10.1146/annurev-med-122313-085916.

Pasquinelli AE: MicroRNAs and their targets: recognition, regulation and an emerging reciprocal relationship. Nature reviews Genetics 2012, 13(4):271-282.

Passaquin AC, Metzinger L, Léger JJ, Warter JM, Poindron P: Prednisolone enhances myogenesis and dystrophin-related protein in skeletal muscle cell cultures

from mdx mouse. *J Neurosci Res* 35: 363-372, 1993.

Pisani A, Visciano B, Roux GD, Sabbatini M, Porto C, Parenti G, Imbriaco M. Enzyme replacement therapy in patients with Fabry disease: state of the art and review of the literature. Mol Genet Metab. 2012 Nov;107(3):267-75.

Porto C, Pisani A, Rosa M, Acampora E, Avolio V, Tuzzi MR, Visciano B, Gagliardo C, Materazzi S, la Marca G, Andria G, Parenti G. Synergy between the pharmacological chaperone 1-deoxygalactonojirimycin and the human recombinant alpha-galactosidase A in cultured fibroblasts from patients with Fabry disease. J Inherit Metab Dis. 2012 May;35(3):513-20

Porto C, Cardone M, Fontana F, Rossi B, Tuzzi MR, Tarallo A, Barone MV, Andria G, Parenti G. The pharmacological chaperone N-butyldeoxynojirimycin enhances enzyme replacement therapy in Pompe disease fibroblasts. Mol Ther. 2009 Jun;17(6):964-71

Raben N, Nagaraju K, Lee E, Kessler P, Byrne B, Lee L, LaMarca M, King C, Ward J, Sauer B, Plotz P. Targeted disruption of the acid alpha-glucosidase gene in mice causes an illness with critical features of both infantile and adult human glycogen storage disease type II. J Biol Chem. 1998 Jul 24;273 (30):19086-92

Raben N, Danon M, Gilbert AL, Dwivedi S, Collins B, Thurberg BL, Mattaliano RJ, Nagaraju K, Plotz PH: Enzyme replacement therapy in the mouse model of Pompe disease. *Mol Genet Metab* 2003, 80:159-169.

Rombach SM, Smid BE, Bouwman MG, Linthorst GE, Dijkgraaf MG, Hollak CE. Long term enzyme replacement therapy for Fabry disease: effectiveness on kidney, heart and brain. Orphanet J Rare Dis. 2013 Mar 25;8:47

Rong H, Liu TB, Yang KJ, Yang HC, Wu DH, Liao CP, Hong F, Yang HZ, Wan F, Ye XY et al: MicroRNA-134 plasma levels before and after treatment for bipolar mania. Journal of psychiatric research 2011, 45(1):92-95.
Schiffmann R, Kopp JB, Austin HA 3rd, Sabnis S, Moore DF, Weibel T, Balow JE, Brady RO. Enzyme replacement therapy in Fabry disease: a randomized controlled trial. JAMA. 2001 Jun 6;285(21):2743-9

Schaefer RM, Tylki-Szymańska A, Hilz MJ. Enzyme replacement therapy for Fabry disease: a systematic review of available evidence. Drugs. 2009 Nov 12;69(16):2179-205

Schweicker WD, Hall J: ICU-acquired weakness. *Chest* 131: 1541-1549, 2007.

Shukla GC, Singh J, Barik S: MicroRNAs: Processing, Maturation, Target Recognition and Regulatory Functions. Molecular and cellular pharmacology 2011, 3(3):83-92.

Slonim AE, Bulone L, Ritz S, Goldberg T, Chen A, Martiniuk F: Identification of two subtypes of infantile acid maltase deficiency. *J Pediatr* 2000, 137:283-285.

Spada M, Pagliardini S, Yasuda M, Tukel T, Thiagarajan G, Sakuraba H, Ponzone A, Desnick RJ. High incidence of later-onset fabry disease revealed by newborn screening. Am J Hum Genet. 2006 Jul;79(1):31-40

Tanaka M, Ohashi T, Kobayashi M, Eto Y, Miyamura N, Nishida K, Araki E, Itoh K, Matsushita K, Hara M, Kuwahara K, Nakano T, Yasumoto N, Nonoguchi H, Tomita K. Identification of Fabry's disease by the screening of alpha-galactosidase A activity in male and female hemodialysis patients. Clin Nephrol. 2005 Oct;64(4):281-7

Thaloor D, Miller KJ, Gephart J, Michell PO, Pavlath GK: Systemic administration of the NF-kB inhibitor curcumin stimulates muscle regeneration after traumatic injury. AM J Physiol 1999, 277:C320-C329.

Thurberg BL, Lynch Maloney C, Vaccaro C, Afonso K, Tsai AC, Bossen E, Kishnani PS, O'Callaghan M: Characterization of pre- and post-treatment pathology after enzyme replacement therapy for Pompe disease. *Lab Invest* 2006, 86:1208-1220.

Van den Hout H, Reuser AJ, Vulto AG, Loonen MC, Cromme-Dijkhuis A, Van der Ploeg AT. Recombinant human alpha-glucosidase from rabbit milk in Pompe patients. Lancet. 2000 Jul 29;356(9227):397-8

van Capelle CI, Winkel LP, Hagemans ML, Shapira SK, Arts WF, van
Doorn PA, Hop WC, Reuser AJ, Ploeg AT van der: Eight years experience with enzyme replacement therapy in two children and one adult with Pompe disease. *Neuromuscul Disord* 2008, 18:447-452.

van der Beek NA, de Vries JM, Hagemans ML, Hop WC, Kroos MA, Wokke JH, de Visser M, van Engelen BG, Kuks JB, van der Kooi AJ, Notermans NC, Faber KG, Verschuuren JJ, Reuser AJ, van der Ploeg AT, van Doorn PA. Clinical features and predictors for disease natural progression in adults with Pompe disease: a nationwide prospective observational study. Orphanet J Rare Dis. 2012 Nov 12;7:88

van der PLoeg AT, Reuser AJ. Pompe's disease. Lancet. 2008, Oct11;372(9646):1342-53.

Vill K, Schessl J, Teusch V, Schroeder S, Blaschek A, Schoser B, Muller-Felber W. Muscle ultrasound in classic infantile and adult Pompe disease: A useful screening tool in adults but not in infants. Neuromuscul Disord. 2014 Oct 22. pii: S0960-8966(14)00662-2

Young SP, Zhang H, Corzo D, Thurberg BL, Bali D, Kishnani PS, Millington DS. Long-term monitoring of patients with infantile-onset Pompe disease on enzyme replacement therapy using a urinary glucose tetrasaccharide biomarker. Genet Med. 2009 Jul;11(7):536-41

Wang GK, Zhu JQ, Zhang JT, Li Q, Li Y, He J, Qin YW, Jing Q: Circulating microRNA: a novel potential biomarker for early diagnosis of acute myocardial infarction in humans. European heart journal 2010, 31(6):659-666.

Weidemann F, Niemann M, Störk S, Breunig F, Beer M, Sommer C, Herrmann S, Ertl G, Wanner C. Long-term outcome of enzyme-replacement therapy in advanced Fabry disease: evidence for disease progression towards serious complications. J Intern Med. 2013 Oct;274(4):331-41

Wyatt K, Henley W, Anderson L, Anderson R, Nikolaou V, Stein K, Klinger L, Hughes D, Waldek S, Lachmann R, Mehta A, Vellodi A, Logan S. The effectiveness and cost-effectiveness of enzyme and substrate replacement therapies: a longitudinal cohort study of people with lysosomal storage disorders. Health Technol Assess. 2012;16(39):1-543.

Whybra C, Bähner F, Baron K. Measurement of disease severity and progression in Fabry disease. In: Mehta A, Beck M, Sunder-Plassmann G, editors. Fabry Disease: Perspectives from 5 Years of FOS. Oxford: Oxford PharmaGenesis; 2006. Chapter 32

Zhou D, Birkenmeier CS, Williams MW, Sharp JJ, Barker JE, Bloch RJ: Small, membrane-bound, alternatively spliced forms of ankyrin 1 associated with the sarcoplasmic reticulum of mammalian skeletal muscle. J Cell Biol 1997, 136:621-631.